WISC

UC-427

UNIVERSITY OF WISCONSIN • MADISON, WISCONSIN

PLASMA PHYSICS

46
5-10-95

LOWER HYBRID ACCESSIBILITY IN A LARGE, HOT REVERSED FIELD PINCH

ROBIN ANN DZIUBEK

DOE/ER/53212-256

February 1995

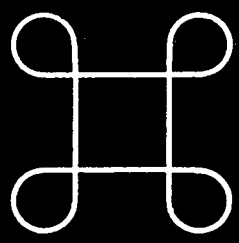

ONSIN

NOTICE

Printed in the United States of America
Available from
National Technical Information Service
U.S. Department of Commerce
5285 Port Royal Road
Springfield, VA 22161

NTIS Price codes
Printed copy: A04
Microfiche copy: A01

LOWER HYBRID ACCESSIBILITY IN A LARGE, HOT REVERSED FIELD PINCH

by

ROBIN ANN DZIUBEK

A thesis submitted in partial fulfillment of the
requirements for the degree of

Master of Science
(Physics)

at the
UNIVERSITY OF WISCONSIN - MADISON
1994

i. Abstract

Recent theoretical and experimental results indicate that driving a current in the outer radius of an RFP suppresses sawtooth activity and increases particle and energy confinement times. One candidate for a form of steady state current drive is the slow wave at the lower hybrid frequency. Here, the accessibility of such a wave in an RFP plasma is investigated theoretically, with focus on the RFX machine (R = 2.0m, a = 0.457m, I_p < 2MA) of Padua, Italy. To drive current, the slow wave with frequency between 1.0 - 1.5 GHz is considered where optimal Landau damping is desired at r/a ~ 0.7. By numerically determining the values of the wave's perpendicular index of refraction which satisfy the hot plasma dispersion relation, regions of propagation and evanescence can be found. The path of the wave can then be traced over a contour map of these regions so that accessibility can be clearly seen. The possibility of mode conversion events can be ascertained by plotting the values of the perpendicular index of refraction for the fast and slow wave and observing convergence points. To locate regions of maximum Landau damping, a technique developed by Stix was adapted for use with the slow wave in an RFP plasma. Results show that the slow wave is accessible to the target region without mode conversion so long as the value of the parallel index of refraction is correctly chosen at the edge of the plasma. Landau damping can also be optimized with this method.

In an RFP, two to twenty percent of the electron population consists of fast electrons. Because this species alters the total electron distribution function and raises the effective temperature in the outer regions of the plasma, its presence is expected to shift the location of ideal Landau damping. By extrapolating hot

electron data from the Madison Symmetric Torus (MST) to RFX, the hot plasma code was adapted to accommodate these electrons and determine their significance. It is found that the presence of this species does not affect the accessibility of the wave. However, the phase velocity of the wave needs to increase by 6% to maintain optimal damping.

ii. Acknowledgments

I would like to express my thanks to all those who helped with this research. In particular, my gratitude to my advisor, Professor Samuel Hokin for offering me this opportunity as well as for his advice and suggestions. Special thanks to Ebo Uchimoto for the enlightening conversations and for the graphs shown in Figures 13 and 15. I would also like to acknowledge the support and inspiration from the entire plasma physics group at UW - Madison, particularly Brett Chapman, Paul Fontana, Edwardo Fernandez, Kevin Mirus, Chuang Ren, Matt Stoneking, and Carl Sovenic. Most especially, I would like to thank my fiancée, David Olson, for his eternal patience, support, interest, and understanding.

This work supported by the U.S. Department of Energy.

I. Introduction

Reversed field pinch (RFP) plasmas are characterized by comparable toroidal and poloidal magnetic field components ($B_\phi \sim B_\theta$) where both elements of the field are powered by a poloidal field circuit driving a toroidal current. Poloidal current is partly driven by the dynamo mechanism which is theorized to be caused by the interaction of fluctuations in fluid flow velocity and magnetic field.[1] Unfortunately, the effects of the dynamo extend beyond current generation to include mode locking, turbulence generation, and enhanced particle and energy transport.[2,3,4] Control of the dynamo, then, is critical to the improvement of an RFP.

Recent experiments suggest that dynamo activity can be suppressed by externally driving a poloidal current in the plasma. Using the three dimensional MHD code, DEBS[5], Ho simulated the addition of an applied loop voltage and electrostatic helicity injection to an RFP plasma.[6] The resulting magnetic configuration was stable to MHD activity driven by currents. Sarff[7] introduced an inductive poloidal electric field into the plasma in the Madison Symmetric Torus (MST)[8] RFP device in order to drive an auxiliary poloidal current. The driven current was shown to flatten the current density profile, suppress sawtooth activity, and double the energy confinement. In the search for a form of steady state current drive, Shiina[9] and Ishii[10] performed theoretical investigations of current drive for the TPE-RX project using the fast magnetosonic wave ($\omega_{ci} < \omega < \omega_{LH}$, where ω_{ci} is the ion cyclotron frequency and ω_{LH} is the lower hybrid frequency). They favor the fast wave over the slow wave because of its high parallel phase velocity, which is predicted to allow the wave to reach the interior of a high beta RFP plasma. Their

calculations show that the fast wave is an efficient current driver in the high-density regions of the plasma and a strong candidate for creating a dynamo-free RFP.

Unlike the fast wave, the slow wave possesses the advantages of a higher frequency and a simpler antenna design. While accessibility to the core may be limited, investigation by Uchimoto[11], using the cold plasma dispersion relation and an RFP-adapted version of the Brambilla raytracing code[12] showed that the wave can get deep enough into the plasma to reach a target region at $r/a = 0.7$. According to numerical simulations run with DEBS, currents added to this region stabilize a larger portion of the plasma than if current were added at other radii. This makes the slow wave an attractive option.

This paper attempts to address some of the gaps in investigations of lower hybrid wave accessibility in an RFP. It is a theoretical exploration of the accessibility of a high frequency slow wave ($f \approx$ 1.0-1.5 GHz) launched into the RFX RFP[13] of Padua, Italy. This machine is characterized by larger dimensions ($R = 2.0$ m, $a = 0.457$ m) and a larger maximum current ($I < 2$ MA) than other machines. It should be noted that RFX has not actually achieved a 2 MA current to date. However, for the purpose of examining this subject at higher temperatures, we shall extrapolate the present performance of MST and RFX up to this current. RFX will run with a magnetic field strength of 8.75 kG at 2 MA, placing the lower hybrid frequency at about 0.57 GHz. In order to avoid strong ion plasma resonances, a frequency of 2.0 to 2.5 times the lower hybrid frequency was chosen. Hokin[14], has investigated the feasibility of using lower hybrid current drive in a 2 MA RFX in order to maintain 10% beta. (Beta, which is a measure of plasma energy to magnetic field energy, decreases in RFP's as I/N increases according to the empirical scaling $\beta = \beta_{max}[(I/N)/2]^{-0.6}$.) In the course of his work, he developed some plasma parameters using the fit for beta and the relation

$$T = \frac{3}{2}\beta\frac{I}{N}I \quad (1)$$

where T is the temperature in keV. Here I is the toroidal current and $N = \pi a^2\langle n\rangle$ where a is minor radius and $\langle n\rangle$ is the volume averaged density. These parameters will also be used for this work and are reproduced in Table 1.

The hot plasma dispersion relation is used in this project to investigate the effect of high temperature on the accessibility of the slow wave. Assuming an infinite plasma with a fixed temperature and density and a wave of fixed frequency and parallel index of refraction, values of the perpendicular index of refraction are determined using root solving methods. The plasma temperature and density and wave parallel index of refraction are then changed to correspond to a radial step by the wave deeper into the plasma and the next root is found. In this way, effects such as cutoff, mode conversion, and optimization of Landau damping are explored. It is also possible to use this method to observe the effects of fast electrons, which make up 10 - 20% of the edge electron density in an RFP.[15,16]

The paper is organized as follows: Section II describes the hot plasma dispersion relation used and lists assumptions made about the electron and ion species in RFX. In Section III, initial accessibility studies for an electron/ion plasma are performed. The method used to find regions of optimal Landau damping is covered in Section IV. The addition of a fast electron species is discussed in Section V. Section VI presents conclusions and speculates on future work.

II. The Hot Plasma Dispersion Relation

In order to explore the accessibility conditions of the lower hybrid wave, the hot plasma dispersion relation developed by Swanson[17] is used. This dispersion relation is derived assuming a drifting, anisotropic Maxwellian distribution of particles of the form

$$f_0\left(v_\perp, v_{//}\right) = \left(\frac{1}{\pi}\right)^{3/2} \frac{1}{v_{t//} v_{t\perp}^2} exp\left[-\frac{\left(v_{//} - v_0\right)^2}{v_{t//}^2} - \frac{v_\perp^2}{v_{t\perp}^2} \right] \tag{2}$$

where $v_{t//}$ is the longitudinal thermal velocity ($v_{t//}^2 = 2T_{//}/m$) and $v_{t\perp}$ is the transverse thermal velocity ($v_{t\perp}^2 = 2T_\perp/m$). The parallel drift velocity of each species is denoted by v_0. The magnetic field, $\boldsymbol{B}$, is assumed to lie along the z-axis of the local Cartesian coordinate system which is pictured in Figure 1. The wave numbers, $k_x = k_\perp \cos\psi$, $k_y = k_\perp \sin\psi$, and k_z are also pictured, where ψ is the angle between the projection of $\boldsymbol{k}$ into the x,y-planes and the x-axis.

The resulting wave equation is

$$\begin{pmatrix} \kappa_{xx} - k_z^2 - k_y^2 & \kappa_{xy} + k_x k_y & \kappa_{xz} + k_x k_z \\ \kappa_{yx} + k_y k_x & \kappa_{yy} - k_z^2 - k_x^2 & \kappa_{yz} + k_y k_z \\ \kappa_{zx} + k_z k_x & \kappa_{zy} + k_z k_y & \kappa_{zz} - k_x^2 - k_y^2 \end{pmatrix} \begin{pmatrix} E_x \\ E_y \\ E_z \end{pmatrix} = 0. \tag{3}$$

Here, $\kappa_{ij} = (\omega/c)^2 K_{ij}$, where the K_{ij} are elements of the hot plasma dielectric tensor

$$\underline{\underline{\boldsymbol{K}}} = \begin{pmatrix} K_1 + K_0 \sin^2\psi & K_2 - K_0 \cos\psi \sin\psi & K_4 \cos\psi + K_5 \sin\psi \\ -K_2 - K_0 \cos\psi \sin\psi & K_1 + K_0 \cos^2\psi & K_4 \sin\psi - K_5 \cos\psi \\ K_4 \cos\psi - K_5 \sin\psi & K_4 \sin\psi + K_5 \cos\psi & K_3 \end{pmatrix} \tag{4}$$

in which the six tensor coefficients are expressed below:

$$K_0 = 2\sum_j \frac{\omega_{pj}^2 e^{-\lambda_j}}{\omega k_z v_{tllj}} \sum_{n=-\infty}^{\infty} \lambda_j (I_n - I_n') \times \left[\left(1 - \frac{k_z v_{0j}}{\omega} \right) Z(\zeta_{nj}) + \frac{k_z v_{tllj}}{\omega} \left(1 - \frac{T_{\perp j}}{T_{llj}} \right) \frac{Z'(\zeta_{nj})}{2} \right] \quad (5)$$

$$K_1 = 1 + \sum_j \frac{\omega_{pj}^2 e^{-\lambda_j}}{\omega k_z v_{tllj}} \sum_{n=-\infty}^{\infty} \frac{n^2 I_n}{\lambda_j} \times \left[\left(1 - \frac{k_z v_{0j}}{\omega} \right) Z(\zeta_{nj}) + \frac{k_z v_{tllj}}{\omega} \left(1 - \frac{T_{\perp j}}{T_{llj}} \right) \frac{Z'(\zeta_{nj})}{2} \right] \quad (6)$$

$$K_2 = i\sum_j \frac{\varepsilon_j \omega_{pj}^2 e^{-\lambda_j}}{\omega k_z v_{tllj}} \sum_{n=-\infty}^{\infty} n(I_n - I_n') \times \left[\left(1 - \frac{k_z v_{0j}}{\omega} \right) Z(\zeta_{nj}) + \frac{k_z v_{tllj}}{\omega} \left(1 - \frac{T_{\perp j}}{T_{llj}} \right) \frac{Z'(\zeta_{nj})}{2} \right] \quad (7)$$

$$K_3 = 1 - \sum_j \frac{\omega_{pj}^2 e^{-\lambda_j}}{\omega k_z^2 v_{tllj}^2} \sum_{n=-\infty}^{\infty} I_n(\omega + n\omega_{cj}) \times \left\{ \frac{2n\omega_{cj} T_{llj} v_{0j}}{\omega T_{\perp j} v_{tllj}} Z(\zeta_{nj}) + \left[1 + \frac{n\omega_{cj}}{\omega} \left(1 - \frac{T_{llj}}{T_{\perp j}} \right) \right] Z'(\zeta_{nj}) \right\} \quad (8)$$

$$K_4 = \sum_j \frac{k_\perp \omega_{pj}^2 e^{-\lambda_j}}{k_z \omega \omega_{cj}} \sum_{n=-\infty}^{\infty} \frac{n I_n}{\lambda_j} \times \left\{ \frac{n\omega_{cj} v_{0j}}{\omega v_{tllj}} Z(\zeta_{nj}) + \left[\frac{T_{\perp j}}{T_{llj}} - \frac{n\omega_{cj}}{\omega} \left(1 - \frac{T_{\perp j}}{T_{llj}} \right) \right] \frac{Z'(\zeta_{nj})}{2} \right\} \quad (9)$$

$$K_5 = i\sum_j \frac{k_\perp \varepsilon_j \omega_{pj}^2 e^{-\lambda_j}}{k_z \omega \omega_{cj}} \sum_{n=-\infty}^{\infty} (I_n - I_n') \times \left\{ \frac{n\omega_{cj} v_{0j}}{\omega v_{tllj}} Z(\zeta_{nj}) + \left[\frac{T_{\perp j}}{T_{llj}} - \frac{n\omega_{cj}}{\omega} \left(1 - \frac{T_{\perp j}}{T_{llj}} \right) \right] \frac{Z'(\zeta_{nj})}{2} \right\} \quad (10)$$

In the above expressions, the summation over j is a summation over species, ω_p are the plasma frequencies, ω_c are the cyclotron frequencies, and ω is the wave frequency. The λ_j are Larmor radius length scales equal to $(1/2)k_\perp^2 \rho_{Lj}^2$, where ρ_{Lj} is

the Larmor radius of the species. I_n and I_n' are the modified Bessel function of the *nth* order and its derivative, where the argument for each is λ_j. Z and Z' are the Fried-Conte dispersion function and its derivative with the argument $\zeta_{nj} = \left(\omega + n\omega_{cj} - k_z v_{0j}\right)/k_z v_{tllj}$. The sign of the charge of each species is represented by ε_j.

By setting $\psi = 0$ (the equivalent of performing a rotation of the coordinate system about the *z*-axis), the relation can be simplified to

$$\left[\gamma\left(\gamma - K_0 + n_\perp^2\right) + K_2^2\right]K_3 + n_\perp^2\left[\left(\gamma - K_0 + n_\perp^2\right)K_1 - K_2^2\right] + K_4\left(\gamma - K_0 + n_\perp^2\right)\left(2n_\perp n_{ll} + K_4\right) - K_5\left[\gamma K_5 + 2K_2\left(n_\perp n_{ll} + K_4\right)\right] = 0 \qquad (11)$$

where $\gamma = n_{ll}^2 - K_1$. The wave numbers have all been replaced with indices of refraction through the relation $\boldsymbol{k} = \boldsymbol{n}\omega/c$. Note that if a non-drifting, isotropic Maxwellian distribution of particles is assumed ($v_0 \to 0$, $T_{ll} = T_\perp$) with temperature approaching zero, the dispersion relation resembles its cold plasma analog. The dielectric tensor elements K_0, K_4, and K_5 all vanish while K_1, K_2, and K_3 take on the values of the *S*, *-iD*, and *P* coefficients of the standard cold dielectric tensor developed by Stix[18].

In order to use this relation to research accessibility, it was programmed as a FORTRAN-77 code in a UNIX background. The code uses an adapted form of DZANLY[19], an IMSL rootsolving routine which employs Müller's method[20] to find roots. This method follows the gradient of the function in the complex plane until absolute zero is reached, at which point it has found a root. Two of the subroutines - the plasma dispersion function and modified Bessel function - are pivotal points in the program and deserve special attention here.

The plasma dispersion function (Z function) is defined as

$$Z(\zeta) = i\sqrt{\pi}\, exp\left(-\zeta^2\right) - 2S(\zeta) \tag{12}$$

in which $S(\zeta)$ is Dawson's function:

$$S(\zeta) = exp\left(-\zeta^2\right)\int_0^{\zeta} dz\, exp\left(z^2\right). \tag{13}$$

For the purpose of this work, it was necessary to model the dispersion function for cases of large and small $|\zeta|$. In the latter case, Dawson's integral could be directly determined without the threat of machine overflow. In the case of large $|\zeta|$, however, it was necessary to apply the asymptotic expansion for the function which has been defined as

$$Z(\zeta) = i\sqrt{\pi}\, exp\left(-\zeta^2\right) - \zeta^{-1}\left(1 + \frac{1}{2\zeta^2} + \frac{3}{4\zeta^4} + \frac{15}{8\zeta^6} + \ldots\right). \tag{14}$$

The routine uses the first four of the terms in the expansion. The resulting function, ZFUNC, is plotted in Figure 2.

The modified Bessel function is of particular concern due to its asymptotic nature. The standard numerical routine employs the recursion relation

$$I_{n-1}(\lambda) - I_{n+1}(\lambda) = \frac{2n}{\lambda} I_n(\lambda) \tag{15}$$

whose numerical solution involves a successive normalization of each term. Unfortunately, as $|\lambda|$ grows large (which it does for ion terms), limited computer precision forces the normalizing factor to zero. In order to avoid this problem, the

code determines the function value in three different regions. For small values of $|\lambda|$, the IMSL routine DCBINS[21] is applied which uses the recursion relation above. For large values of $|\lambda|$, the code uses one of two asymptotic expansions[22] for the modified Bessel function. For small n,

$$I_n(\lambda) \approx \frac{e^{\lambda}}{\sqrt{2\pi\lambda}}\left\{1-\frac{\mu-1}{8\lambda}+\frac{(\mu-1)(\mu-9)}{2!(8\lambda)^2}-\frac{(\mu-1)(\mu-9)(\mu-25)}{3!(8\lambda)^3}+\ldots\right\} \tag{16}$$

is used, where $\mu = 4n^2$ and the series is carried out to twenty-five terms. For large n, a slightly more complex expression is required

$$I_n(nz) \approx \frac{1}{\sqrt{2\pi n}}\frac{e^{n\eta}}{\left(1+z^2\right)^{1/4}}\left\{1+\sum_{k=1}^{\infty}\frac{u_k(t)}{n^k}\right\} \tag{17}$$

to which the following definitions apply:

$$z = \lambda/n \qquad t = 1/\sqrt{1+z^2} \qquad \eta = \sqrt{1+z^2} + ln\frac{z}{1+\sqrt{1+z^2}}$$

$$u_0(t) = 1 \tag{18}$$

$$u_{k+1}(t) = \frac{1}{2}t^2\left(1-t^2\right)u_k'(t)+\frac{1}{8}\int_0^t\left(1-5t^2\right)u_k(t)dt$$

and the first four terms of this series are used. The function, BES, is shown in Figure 3.

Several assumptions were made about the electron and ion distributions of RFX. Ions were taken to be protons. Quasineutrality was upheld by setting $n_e = n_i$, where n_j represents density. The ion and electron temperatures were set equal to each other since these two species are assumed to be collisionally coupled in

RFX. The parallel and perpendicular temperatures of each species were also set equal. Lastly, it was assumed that neither species has a significant drift velocity so that v_0 could be set to zero. For the majority of the investigation covered in this paper, the projected temperature and density of RFX at $I/N = 6\times10^{-14}\, A\cdot m$ were used as plasma parameters. In the code, the density profile is a typical RFP density profile: $n_e = n_{eo}[1-(r/a)^2]$. Although there are few direct experimental measurements of the temperature profile of an RFP, a quartic relationship is generally accepted to be representative and is used here: $T_e = T_{eo}[1-(r/a)^4]$.

Figures 5, 6, and 7 represent the dependence of $n_\perp$ on density and either temperature, magnetic field, or frequency, respectively. Figure 5 plots the roots of the dispersion relation for increasing density and various values of constant temperature. Although the real part of $n_\perp$ is almost independent of temperature, the slope of the imaginary part becomes steeper and more negative with increasing temperature. This indicates that wave damping becomes stronger with higher temperature. Figure 6 shows roots for different values of constant magnetic field strength. Within a range of 7-8 kG, the dependence of $n_\perp$ on B is more or less monotonically increasing. The imaginary parts are fairly close in value, indicating that damping should not be strongly dependent on magnetic field strength. The dependence shown in Figure 7, on the other hand, is inverse -- $n_\perp$ will decrease as wave frequency increases. Damping is fairly dependent on frequency, with a steeper slope closer to the lower hybrid frequency.

III. Accessibility in an Electron-Ion Plasma

When considering wave accessibility, one is really looking for points in the plasma which are resonances or cutoffs for the wave. A resonance is a point where the index of refraction of the wave passes through infinity. Usually, this occurs when the wave matches frequencies or velocities with some component of the plasma. Wave absorption or reflection can occur here. A cutoff is a point in the plasma where the index of refraction passes through zero and the wave begins to spatially attenuate or grow. Reflection can also occur as the perpendicular index of refraction of the wave decreases and the wave turns to follow the magnetic field. At this point, it mode converts and it is unlikely that its energy will go to the electrons as planned. For these reasons, knowing the location of resonances and cutoffs in the plasma is critical to successful lower hybrid current drive.

Since the $n_{//}$ is set at each step of the plasma, we are really looking for places where the $n_{\perp}$ passes through infinity or zero. The former can be anticipated by comparing the wave frequency to the plasma and cyclotron frequencies of each species of the plasma. As it turns out, the wave should become resonant with the ion plasma frequency at $r/a \approx 0.65$ and, depending upon the value of $n_{//}$, with the electron parallel thermal velocity at deeper points in the plasma. The first of these resonances is very weak and does not impede the travel of the wave. The second is a region of strong Landau damping in the center of the electron velocity distribution function. Landau damping is best described as a collisionless damping of the wave due to a wave-particle interaction. Electrons whose longitudinal thermal velocities match the parallel phase velocity of the wave become trapped in the potential wells of the wave. This trapping allows the wave and particle to

interact and a transfer of energy occurs. Chen[23] explains that, just as an ocean wave traveling slightly faster than a surfboard gives up some of its energy to push the board along, radiofrequency waves moving at higher velocities than the bulk of an electron distribution will deposit energy into the resonant electrons. (This is, of course, the now-famous "surfboard analogy.") It is also possible for a wave moving slower than the bulk of an electron distribution to receive energy from the distribution.

Cutoff can be determined by examining the cold plasma dispersion relation. By using the determinant of the wave equation and requiring that $\omega = 2\sqrt{\omega_{ce}\omega_{ci}}$, or two times the lower hybrid frequency of a high density plasma, an approximate expression for the requirement on $n_{//}$ may be generated:

$$n_{//} \geq \left[\left(1+\omega_{pe}^2/\omega_{ce}^2\right)^{1/2} + \omega_{pe}/\omega_{ce}\right] \tag{19}$$

In general, this limits the travel of a wave with high phase velocity in certain high density regions of the plasma. This condition is absolutely required and independent of temperature. It is not, however, independent of frequency. It can be shown that, as wave frequency is increased, the cutoff will shift to regions of lower density indicating that a high frequency wave will be evanescent in densities accessible to a wave of lower frequency (Figure 8). The cold plasma cutoff is also shown in this figure.

In the case of RFX, the cutoff can be seen by plotting the contours of $n_{\perp}^2 = 0$ on a diagram of $n_{//}$ and density. Figure 9 shows that the cutoff follows that predicted by Equation 19 fairly closely. The region of resonance between the wave and the thermal electrons is also indicated with a dashed line. By assuming that $n_{//}$ increases as the wave steps into the plasma according to $n_{//} = n_{//edge}/(r/a)$, the

exact path of the wave through the plasma may be traced. Laying this trajectory onto the map of the cutoffs, it is possible to observe the position of the wave relative to the cutoff.

One great concern when using the slow wave is that of mode conversion to the fast wave. This event occurs as the wave reaches a resonant or evanescent region in the plasma. If damping is strong, the wave is completely absorbed. However, if damping is weak, there is a possibility of reflection and/or mode conversion. In the latter case, the wave would transmit through or reflect off the layer and emerge as one or more new modes. Obviously, this is extremely undesirable when considering current drive since Landau damping would be altered by the change in the resonance requirements of the wave. If the roots of the dispersion relation are known, mode conversion can be studied by examining the values of $n_\perp$ as density increases. Mode conversion events will appear as turning points of the wave and mode conversion densities can be identified at those points. Figure 10 displays $n_\perp^2$ as a function of density for selected values of $n_{//}$. Note the extra path at the mode conversion density. As the slow wave and fast wave meet at the cutoff, they coalesce into an evanescent mode and propagate until completely damped.

From Figure 10, it can be concluded that mode conversion does not represent a threat to slow wave propagation if $n_{//edge} > 5$. By following the path of a single $n_{//}$, one sees that the conversion density lies relatively deep in the plasma. As the wave moves into the plasma, however, loss of forward velocity forces $n_{//}$ to increase. This 'jump' to a new path moves the applicable mode conversion density deeper into the plasma. As the parallel index of refraction increases again, the cycle continues until it becomes apparent that the wave will never reach a required mode conversion density. This is true, in general, so long as the parallel index of

refraction at the edge is chosen to meet the accessibility condition presented above (Equation 19).

IV. Landau Damping Efficiency

A second criterion in considering the feasibility of lower hybrid current drive in an RFP is that edge conditions optimize electron Landau damping within the area of interest in the plasma. Uchimoto's analysis[11] uses the warm plasma dielectric tensor to determine that Landau damping is optimized in those regions characterized by $v_{ph}/v_{tle} \approx 2.5$ where v_{ph} is the parallel phase velocity of the wave and may be expressed as $v_{ph} = c/n_{\parallel}$. The associated figure[24] is reproduced here by plotting v_{ph}/v_{tle} as a function of temperature and $n_{\parallel}$ (Figure 11). Regions of $v_{ph}/v_{tle} < 2.0$ are characterized by excessive damping while regions of $v_{ph}/v_{tle} > 3.0$ are regions of little damping. Assuming that $n_{\parallel}$ varies as described earlier and that the temperature profile is quartic, it is possible to invoke the "raytracing" technique employed in Figure 9 to plot the path of the wave onto the plot of v_{ph}/v_{tle} contours. By adjusting the starting value of $n_{\parallel}$, the wave can be made to propagate through the outer region of the plasma with little damping until it reaches the region where current drive is desired.

A more quantitative method of determining the region of optimal Landau damping can be found by adapting a technique suggested by Stix[25]. He determines the damping rate, $\Gamma = P/W$, where P is the power per unit volume deposited into the plasma and W is the wave energy density. Power can be expressed as

$$P = -\frac{i\omega}{16\pi} \boldsymbol{E}^* \cdot \underline{\underline{\boldsymbol{K}}} \cdot \boldsymbol{E} + complex \;\; conjugate \qquad (20)$$

where $\boldsymbol{E}$ is the complex amplitude of the wave electric field and $\underline{\underline{\boldsymbol{K}}}$ is the hot plasma dielectric tensor. From cold plasma theory, the polarization of the slow wave is such that $|E_x| >> |E_z|$ and $|E_x| >> |E_y|$, so that $\boldsymbol{E}$ is almost parallel to $\boldsymbol{k}$ and E_y can be effectively ignored. Then,

$$P = -\frac{i\omega}{8\pi}\left[i|E_x|^2 Im(K_1) + 2i\,Re(E_x E_z^*) Im(K_4) + i|E_z|^2 Im(K_3)\right] \tag{21}$$

in which the term dependent on $|E_z|^2$ is power deposited by Landau damping, the term dependent on $|E_x|^2$ is power deposited by transit time magnetic pumping, and the term dependent on $E_x E_z^*$ is a cross term.

The wave energy is, from classical electromagnetic theory,

$$W = \frac{1}{16\pi}\left[\boldsymbol{B}^* \cdot \boldsymbol{B} + \boldsymbol{E}^* \cdot \frac{\partial}{\partial\omega}\left(\omega \underline{\underline{\boldsymbol{K}}}_h\right) \cdot \boldsymbol{E}\right] \tag{22}$$

where $\boldsymbol{B}$ indicates the wave magnetic field and $\underline{\underline{\boldsymbol{K}}}_h$ is the hermitian conjugate of the dielectric tensor. Since the slow wave is predominantly electrostatic, $\boldsymbol{B} \approx 0$ and the equation reduces to

$$W = \frac{1}{16\pi}\left[|E_x|^2 \frac{\partial}{\partial\omega}\left(\omega K_1^*\right) + 2\,Re(E_x E_z^*) \frac{\partial}{\partial\omega}\left(\omega K_4^*\right) + |E_z|^2 \frac{\partial}{\partial\omega}\left(\omega K_3^*\right)\right]. \tag{23}$$

Using the electron elements of the dielectric tensor in the power equation, the electron Landau damping rate is then the Landau damping term of the power

equation divided by the total wave energy. The relative value of E_x is of use here and may be determined from the *y*- and *z*-components of the wave equation:

$$\frac{E_x}{E_z} = -\frac{\left[K_5^2 + \left(K_1 + K_0 - n^2\right)\left(K_3 - n_\perp^2\right)\right]}{\left[K_2 K_5 + \left(K_1 + K_0 - n^2\right)\left(K_4 + n_\perp n_{//}\right)\right]}. \tag{24}$$

By applying Equations 21, 23, and 24 to the definition of Γ, we get the following expression for the Landau damping rate:

$$\Gamma_{LD} \approx 2\omega\left[\frac{Im(K_3)}{\left|E_x/E_z\right|^2 K_1^* + 2Re(E_x/E_z)K_4^* + K_3^*}\right]. \tag{25}$$

Because we have been working in a slab geometry thus far, we cannot maximize the Landau damping rate by taking the derivative with respect to the flux surface area, $d\Gamma_{LD}/d\sigma$. However, it is possible to use the $n_\perp$ determined by the rootsolver to analytically find the region of ideal damping. At the plasma edge, the magnetic field points mainly in the poloidal direction. Therefore, $\boldsymbol{k}_{//} = \boldsymbol{n}_{//}\omega/c$ is along the poloidal field. The perpendicular part of $\boldsymbol{k}$ is in the radial and toroidal directions, with all of $\boldsymbol{k}_\perp$ being in the toroidal direction when the wave is launched at the edge. It is reasonable to assume that $\boldsymbol{k}_\perp$ remains largely toroidal as the wave continues into the plasma, so that the wave makes many toroidal passes per radial step. The fractional power loss per toroidal transit is given by:

$$\frac{1}{P}\frac{dP}{dt}\frac{2\pi R}{v_{g\perp}} = \Gamma_{LD}\frac{2\pi R}{v_{g\perp}}, \tag{26}$$

Here R is major radius and $v_{g\perp} = \partial\omega/\partial k_\perp$ is the group velocity of the wave in the perpendicular direction. If we require that the damping rate be large enough to completely damp the wave in one hundred transits or less, Equation 26 becomes an inequality:

$$\Gamma_{LD} \geq \frac{100 v_{g\perp}}{2\pi R}. \qquad (27)$$

Figure 12 shows the results of applying this logic to RFX for $n_{\parallel edge} = 5.0$ and $n_{\parallel edge} = 6.0$. The region of optimal Landau damping lies at the intersection of the curves representing each side of Equation 27. Since this area lies on either side of $r/a = 0.7$ for the two cases, we assume that $n_{\parallel edge} = 5.5$ is optimal.

The result of all the accessibility conditions discussed in Sections III and IV is a range of parallel indices of refraction to be used as edge conditions for launching a lower hybrid wave into an RFX plasma of known temperature and density. In order to test the validity of the predictions, the data for the case of $I/N = 6\times10^{-14}\,A/m$ with $n_{\parallel edge} = 5.5$ were entered into the RFP-adapted version of the Brambilla raytracing program.[12] Results are shown in Figure 13. The ray enters the plasma at the outboard edge and proceeds around the poloidal plane of the torus until it is completely damped. The power deposition profile shows a sharp spike at $r/a \approx 0.7$, indicating that current was driven in the desired region (Figure 14). With the frequency chosen at $f \approx 2f_{LH}$ to avoid ion plasma resonances, all of the wave power was delivered to the electrons.

Additional simulations were run with different starting values for the parallel index of refraction. Figures 15 and 16 show the results of those cases. Most

notable are the case for $n_{lledge} = 2.6$, in which the wave is a surface mode, and $n_{lledge} = 2.4$, in which the wave is evanescent. These effects occur because of the proximity of the cutoff. When $n_{lledge} = 4$, the wave starts out with a higher phase velocity than if $n_{lledge} = 5.5$ and takes longer to match velocities with the electrons. Therefore, it goes deeper into the plasma before damping. In the opposite sense, if $n_{lledge} = 8$, the wave starts out slower than if $n_{lledge} = 5.5$ and interacts with electrons further from the core. Table 1 shows the optimum values of n_{lledge} for a full density scan of RFX at 2 MA.

V. Fast Electron Effects

One special concern regarding lower hybrid current drive in an RFP involves the larger density of high velocity electrons than would be seen in a tokamak. Measurements on a variety of RFP devices show that these fast electrons make up 2-20% of the edge electron population[15,16]. In MST, Stoneking determined that fast electrons carry nearly all the edge poloidal current, have a parallel temperature comparable to the central electron temperature, and a perpendicular temperature roughly equal to the edge bulk electron temperature[16]. Other groups have reported similar results.

RFX is expected to have fast electron energies in the keV range.[15,26] Located far out on the high velocity tail of the electron distribution, the presence of these electrons fundamentally alters the distribution of the total electron population, creating a slight bump-on-tail distribution. A wave entering the edge of the plasma sees the high temperature of the hot species first and doesn't encounter a significant bulk temperature until it gets deeper into the plasma. This alters the position of the resonant region. The goal of this section is to determine the severity of the effects of the fast electrons.

The fast electrons are relatively collisionless within the plasma and so may be thought of as a separate species from the bulk electrons. Adapting the hot plasma code to accommodate the fast electrons merely involves adding those electrons to the sum over species in each of the *K*-terms of the dielectric tensor (Equations 5-10). Since the parallel temperature of the fast electrons is about equal to the central electron temperature, their temperature remains constant across the minor radius of the plasma. The fast electron drift velocity was

determined by setting $J = en_h v_{oh}$, where J is a model current density profile, n_h is the hot electron density, and v_{oh} is the drift velocity of the hot electrons. For the purpose of this paper, $n_h/n_e = 10\%$. The perpendicular temperature of the fast electrons was set equal to the edge electron temperature. The resulting assumed parallel temperature and density profiles for RFX are shown in Figure 17.

Because the position of the cutoff is, in theory, only dependent upon the local density and magnetic field, the addition of fast electrons is not expected to affect it. On the other hand, the position of the thermal resonance is strongly temperature dependent and should shift further from the core as the local temperature of the outer radii increases. The shift is not severe enough to limit accessibility, however, as can be seen in Figure 18.

With the wave encountering a different distribution of electrons in the outer regions of the plasma, Landau damping should be influenced. The electron distribution is now lopsided, with more electrons in the upper tail of the function. The number of electrons with velocities greater than the wave have increased which should decrease the efficiency of damping in the resonant region chosen in the previous section. The simplest analytical reasoning says that if the wave phase velocity can be altered so that the same number of electrons in the distribution are slower than the wave as there were in the case of the RFP without fast electrons, the efficiency of the damping should be maximized. Figure 19 is an example of this for RFX at $r/a = 0.7$. In this case, the phase velocity must increase by 8% to match efficiency.

It makes sense that the phase velocity of the wave is not expected to change a large amount. The presence of the fast electrons in any region near the edge of the plasma effectively increases the temperature in that region, so it is logical to assume that the area of optimal damping will move further out to the edge. By

using the analytical methods presented in Section IV, the exact effects of this species can be analyzed. The intersection of the curves for Γ_{LD} and $100v_{g\perp}/2\pi R$ have moved to higher *r/a* for $n_{IIedge} = 5.0$ and $n_{IIedge} = 6.0$, amounting to a 6% increase in the optimum wave phase velocity at the edge of the plasma (Figure 20).

VI. Conclusions

The accessibility of the lower hybrid wave in an reversed field pinch device for the purpose of driving an auxiliary poloidal current has been studied using the hot plasma dispersion relation. The slow wave was found to be accessible to $r/a \approx 0.7$ with a cutoff at low values of edge parallel indices of refraction which meet the derived criteria (Equation 19). There is a weak ion plasma resonance at $r/a \approx 0.65$ and a strong electron thermal resonance at deeper points in the plasma. This thermal resonance marks a region of powerful Landau damping in the center of the electron velocity distribution. Mode conversion can be expected in high density regions of the plasma. However, since the value of the parallel index of refraction increases as the wave moves deeper into the plasma, the target density increases as well and it can be seen that the wave will damp out before it reaches a mode conversion point. The addition of a 10% density of fast electrons does not change these accessibility conditions.

By using the imaginary parts of the warm plasma dispersion relation, Uchimoto[11] determined that a region of ideal Landau damping would be reached when $v_{ph}/v_{tle} \approx 2.5$. Direct determination of Landau damping rates by using a technique developed by Stix[25] confirms his calculations. By adapting the hot plasma dispersion relation to accommodate 10% fast electrons, it was determined that the edge parallel phase velocity of the wave should increase by 6% to maintain optimal Landau damping.

From the above, one can see that the use of the lower hybrid wave as a current driver in a large, hot reversed field pinch is feasible. Figures 13 and 14 show ray trajectories and power deposition profiles obtained using a RFP-adapted

version of the Brambilla ray-tracing program[12]. Estimated values of $n_{\|edge}$ for the full density scan of RFX are presented in Table 1.

Although the use of the hot plasma dispersion relation is enlightening, it certainly is not a trivial exercise in computer programming. At high temperatures and densities, it is easy to exceed machine precision capabilities, either by overflowing or underflowing. At resonances, it is impossible for the machine to calculate the true value of the dispersion relation and a great deal of interpretation must be applied to the results. Near resonances, the rootsolver can follow a false gradient and reach its maximum number of iterations before a true root is found. For these reasons, it would be convenient to create a normalized system of variables in order to solve for the roots of the relation. The development of a fully RFP-adapted raytracer coupled with a Fokker-Planck code would also be helpful in further exploring this topic. Evaluation of current drive efficiency, fast electron dispersion rates, and the effects of machine geometry are all important to lower hybrid current drive but are not covered by using the dispersion relation alone. It is likely, however, that further theoretical exploration of this subject will be pre-empted by experimental research. There are already plans to design a series of lower hybrid experiments for MST[27] based upon Uchimoto's predictions[11]. These experiments are expected to test the aptitude of lower hybrid current drive for the purpose of improving confinement in an RFP.

References

1. J.B. Taylor, "Relaxation of toroidal plasmas and generation of reverse magnetic fields", Physical Review Letters **33**, 1139 (1974).

2. A. Almagri, S. Assadi, S.C. Prager, J.S. Sarff, and D.W. Kerst, "Locked modes and magnetic field errors in the Madison Symmetric Torus", Physics of Fluids B **4**, 4080 (1992).

3. G. Fiksel, S.C. Prager, W. Shen, and M. Stoneking, "Measurement of magnetic fluctuation induced energy transport", Physical Review Letters **72**, 1028 (1994).

4. M. Stoneking, S.A. Hokin, S.C. Prager, G. Fiksel, H. Ji, and D. Den Hartog, "Particle transport due to magnetic fluctuations", Physical Review Letters **73**, 549 (1994).

5. D.D. Schnack, D.C. Barnes, Z. Mikic, D.S. Harned, and E.J. Caramana, "Semi-implicit Magnetohydrodynamic calculations", Journal of Computational Physics **70**, 330 (1987).

6. Y.L. Ho, "Numerical simulations of fluctuation suppression via DC helicity injection in a reversed field pinch", Nuclear Fusion **31**, 341 (1991).

7. J.S. Sarff, S.A. Hokin, H. Ji, S.C. Prager, C.R. Sovinec, "Fluctuation and transport in a reversed field pinch by inductive poloidal current drive", Physical Review Letters **72**, 3670 (1994).

8. R.N. Dexter, D.W. Kerst, T.H. Lovell, S.C. Prager, and J.C. Sprott, "The Madison Symmetric Torus", Fusion Technology **19**, 131 (1991).

9. S. Shiina, Y. Kondoh, and H. Ishii, "Partial current drive by a fast magnetosonic wave in a reversed field pinch", Nuclear Fusion **34**, 1473 (1994).

10. H. Ishii, Y. Kondoh, T. Shimada, Y. Hirano, S. Shiina, K. Saito, "MHD equilibrium generation by partial current drive in a reversed field pinch plasma", *Proceedings of the Twentieth European Physical Society Conference on Controlled Fusion and Plasma Physics*, EPS, Lisboa, Vol. 17C, p. 495 (1993).

11. E. Uchimoto, M Cekic, R:W. Harvey, C. Litwin, S.C. Prager, J.S. Sarff, C.R. Sovinec, "Lower-hybrid poloidal current drive for fluctuation reduction in a reversed field pinch", Physics of Plasmas **1**, 3517 (1994).

12. M. Brambilla, "Raytracing of lower hybrid and ion cyclotron waves", Computer Physics Reports **4**, 73 (1986).

13. G. Malesani, *Proceedings of the International School of Plasma Physics Workshop on Physics of Mirrors, Reversed Field Pinches, and Compact Tori*, Varenna, Vol. 1, p. 359 (1987).

14. S.A. Hokin, J.S. Sarff, C.R. Sovinec, E. Uchimoto, "Confinement improvement with RF poloidal current drive in the reversed-field pinch", Nuclear Fusion **34**, 1447 (1994).

15. S. Ortolani, "The behaviour of fast electrons in reversed field pinches", Plasma Physics and Controlled Fusion **34**, 1903 (1992).

16. M.R. Stoneking, "Fast electron generation and transport in a turbulent, magnetized plasma", Ph.D. thesis, University of Wisconsin - Madison (1994).

17. D.G. Swanson, *Plasma Waves*, Academic Press, Inc., Boston (1989).

18. T.H. Stix, *Waves in Plasmas*, American Institute of Physics, New York (1992).

19. *IMSL User's Manual: MATH/LIBRARY v1.0*, IMSL, Inc. (1987).

20. D.E. Müller, "A method for solving algebraic equations using an automatic computer", Mathematical Tables and Aids to Computation **10**, 208 (1956).

21. *IMSL User's Manual: SFUN/LIBRARY v2.0*, IMSL, Inc. (1987).

22. M. Abramowitz, I.A. Stegun, *Handbook of Mathematical Functions*, Dover Publishers, Inc., New York (1965).

23. F.F. Chen, *Plasma Physics and Controlled Fusion, Volume I: Plasma Physics*, Plenum Press, New York (1984).

24. E. Uchimoto, M. Cekic, C. Litwin, S.C. Prager, J.S. Sarff, and C.R. Sovinec, "Lower hybrid current drive in a reversed field pinch", Bulletin of the American Physical Society **38**, 1979 (1993).

25. T.H. Stix, "Fast-wave heating of a two-component plasma", Nuclear Fusion **15**, 737 (1975).

26. S.A. Hokin, A. Almagri, S. Assadi, M. Cekic, B. Chapman, G. Chartas, N. Crocker, M. Cudzinovic, D.J. Den Hartog, R. Dexter, G. Fiksel, R. Fonck, J. Henry, D. Holly, S. Prager, T. Rempel, J. Sarff, E. Scime, W. Shen, J. Sprott, M. Stoneking, C. Watts, "Anomalous ion heating and superthermal electrons in the MST reversed-field pinch", in *Proceedings of the 14th International Conference on Plasma Physics and Controlled Nuclear Fusion*, Wurzburg, p. 539 (1992).

27. M.A. Thomas, M. Cekic, E. Uchimoto, C. Litwin, T.W. Lovell, S.C. Prager, J.S. Sarff, "Conceptual design of a lower-hybrid wave antenna for a reversed field pinch", Bulletin of the American Physical Society **39**, 1539 (1994).

Table 1

I/N	n (x 10^{13}cm^{-3})	T_e (eV)	n_{lledge}
2	15.6	600	5.7 - 7.0
4	7.8	790	5.0 - 6.2
6	5.2	940	4.5 - 5.7
8	3.8	1060	4.4 - 5.4
10	3.1	1140	4.2 - 5.2

Table 1: Temperature and densities for RFX in a conventional density scan. Predicted n_{lledge} are included.

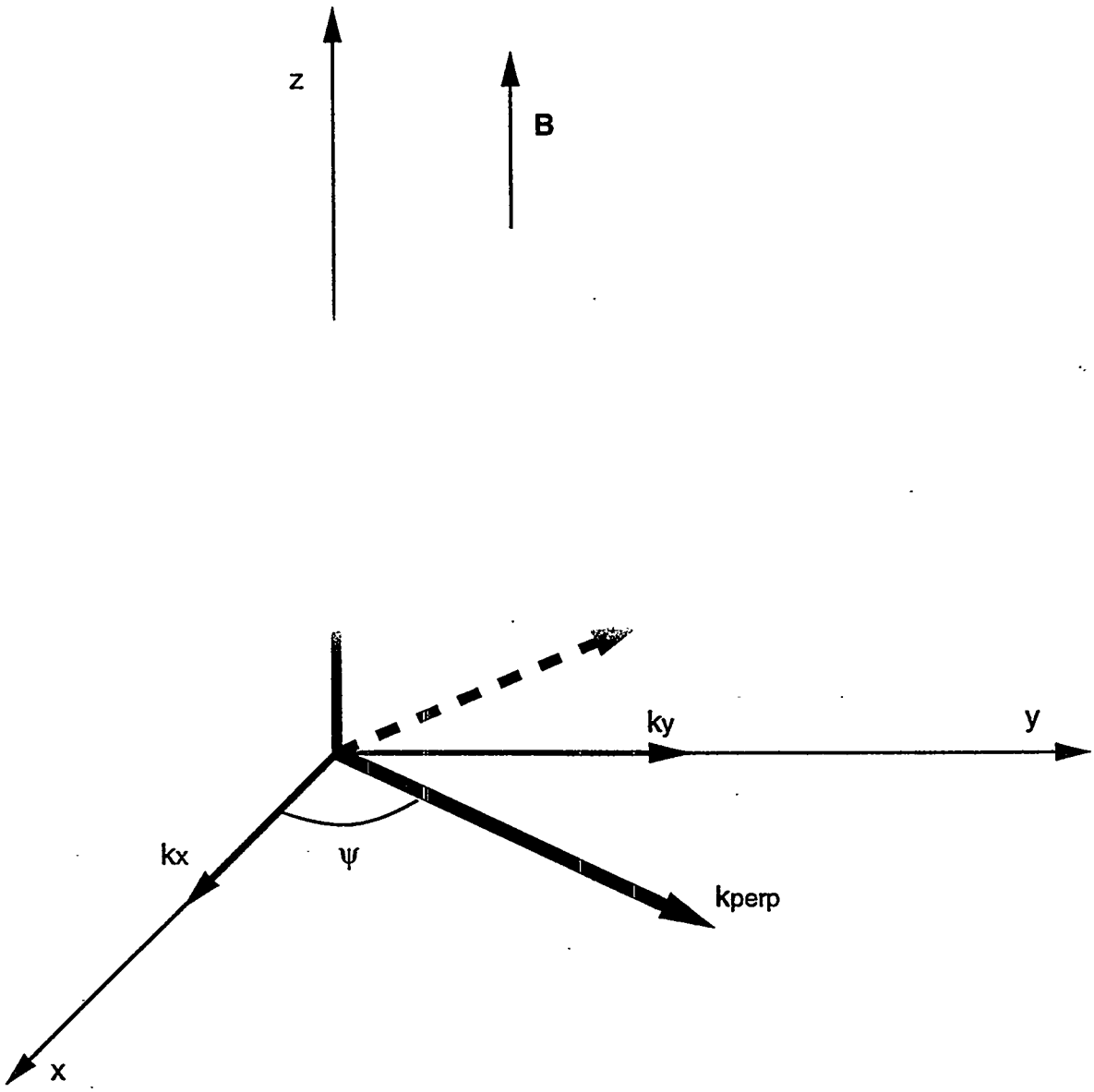

*Figure 1: Local Cartesian coordinate system used to obtain the hot plasma dispersion relation. The magnetic field, **B**, is assumed to lie along the z-axis perpendicular to the x,y-plane. The wave vector, **k**, is represented by components parallel and perpendicular to the magnetic field.*

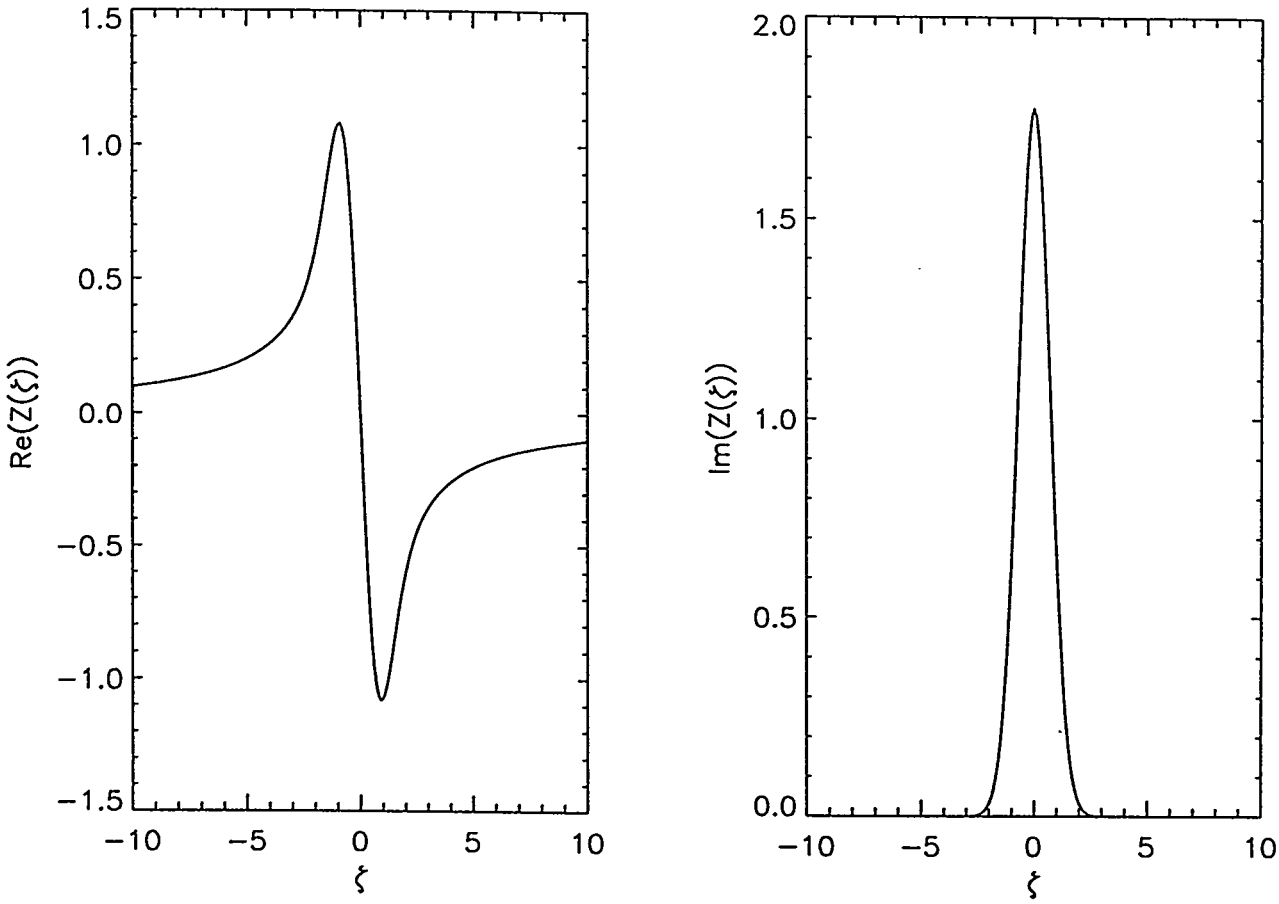

Figure 2: Real and imaginary values of the plasma dispersion function as determined by the function ZFUNC.

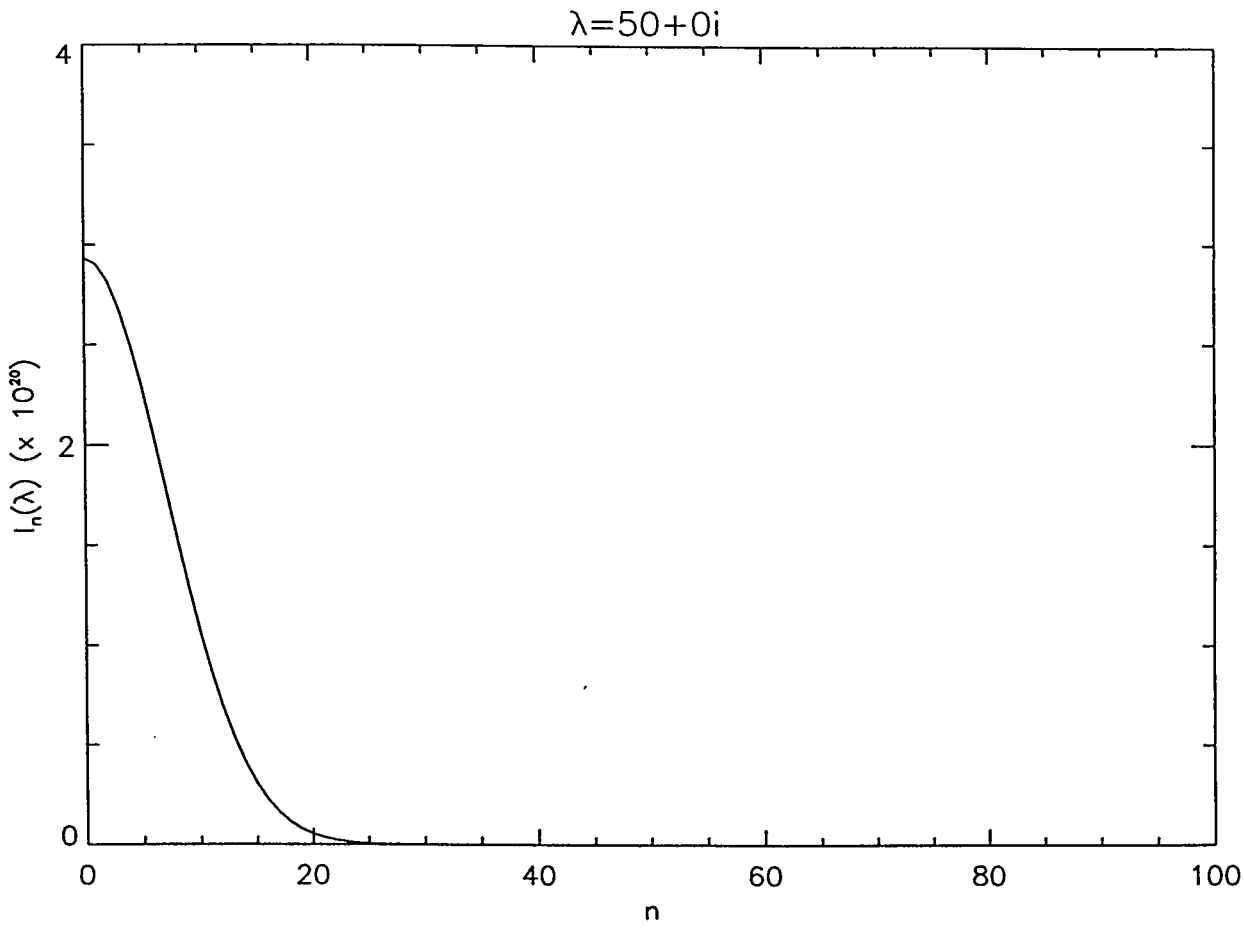

Figure 3: Values of the modified Bessel's function routine, BES, for an arbitrary real argument ($\lambda = 50$).

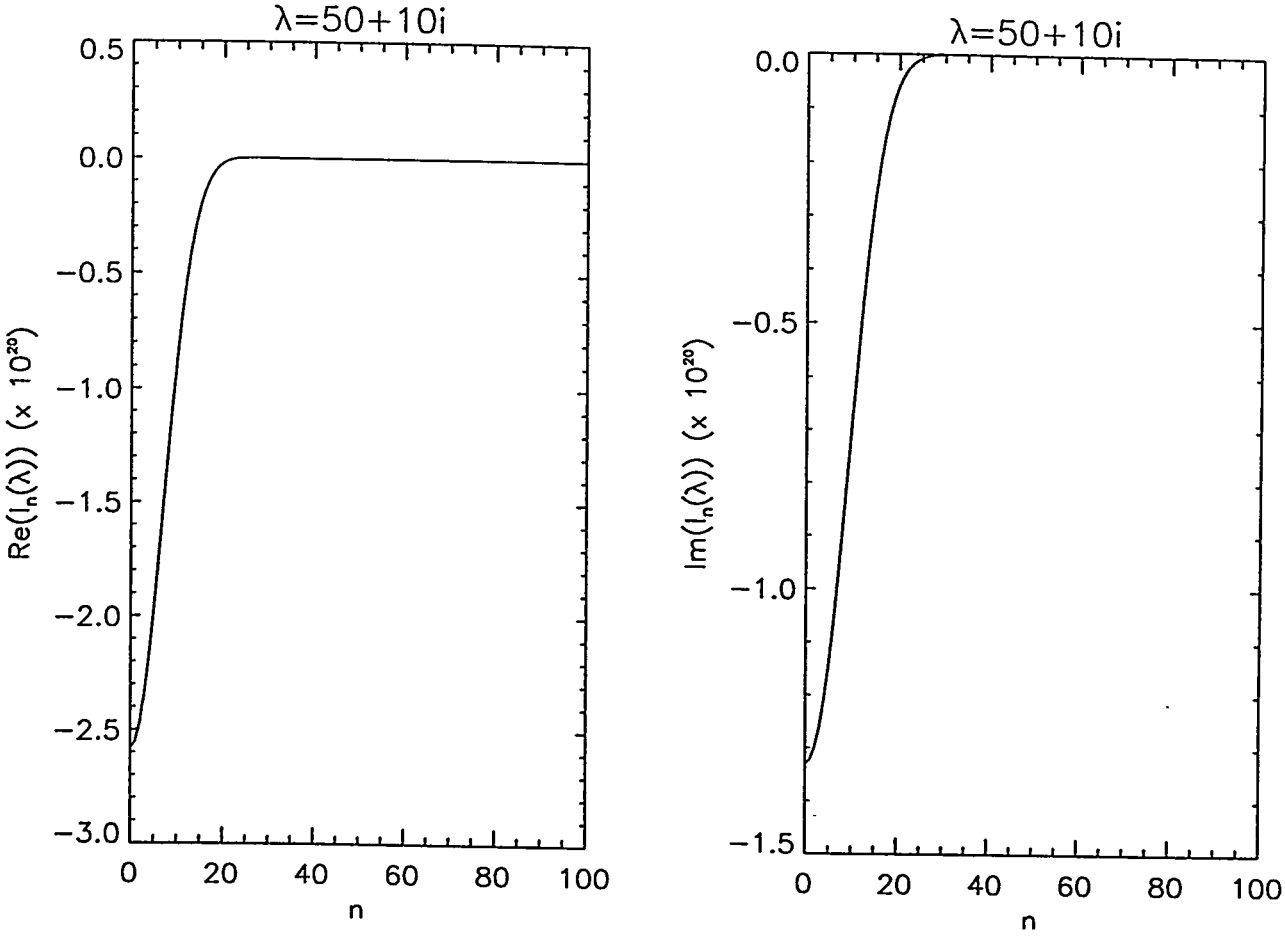

Figure 4: Real and imaginary values of the modified Bessel's function routine, BES, for an arbitrary complex argument ($\lambda = 50 + 10i$).

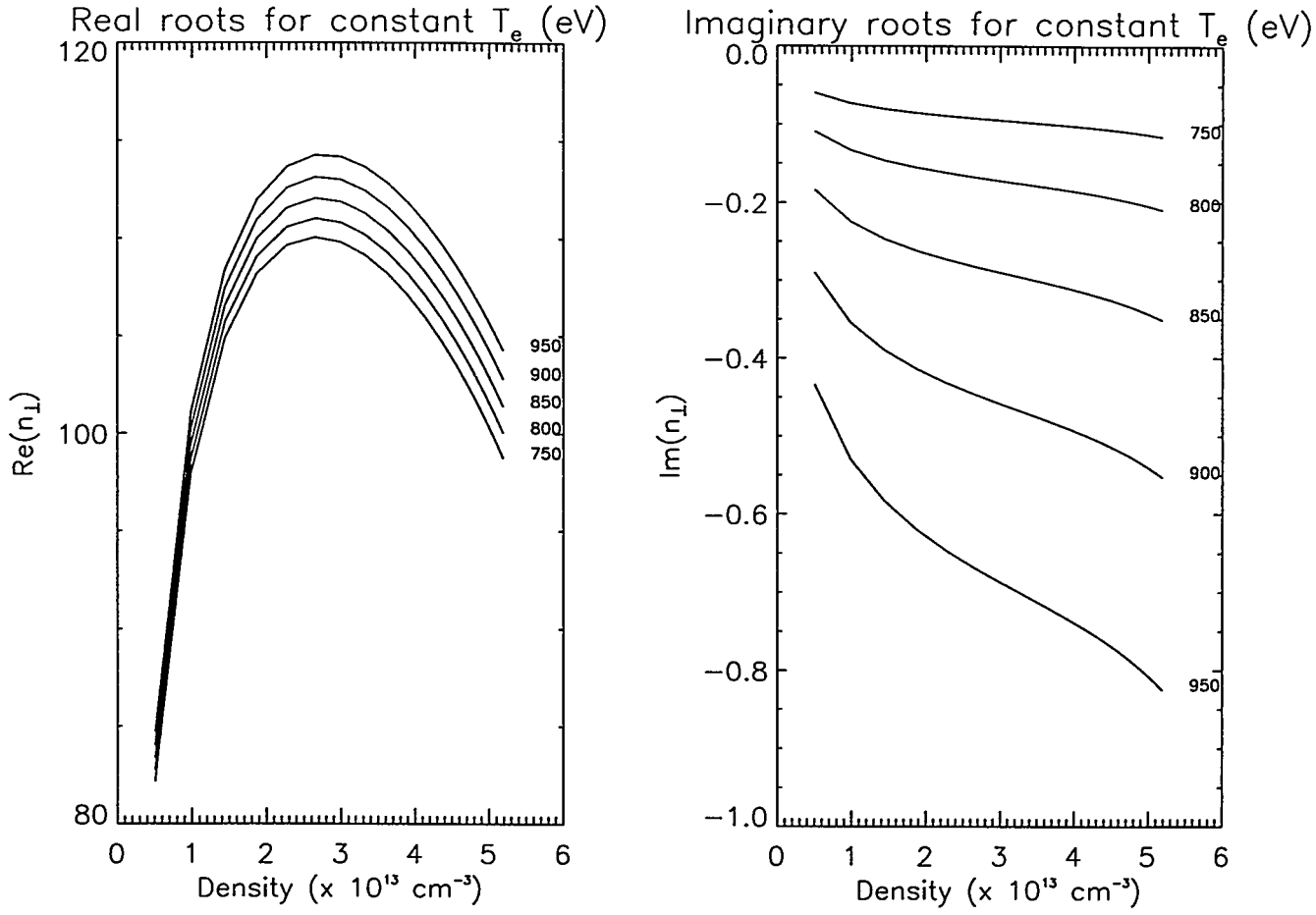

Figure 5: Behavior of the roots of the hot plasma dispersion relation for constant values of temperature. The real part of the function shows little dependence upon temperature. However, the imaginary part shows strong wave damping as temperature increases.

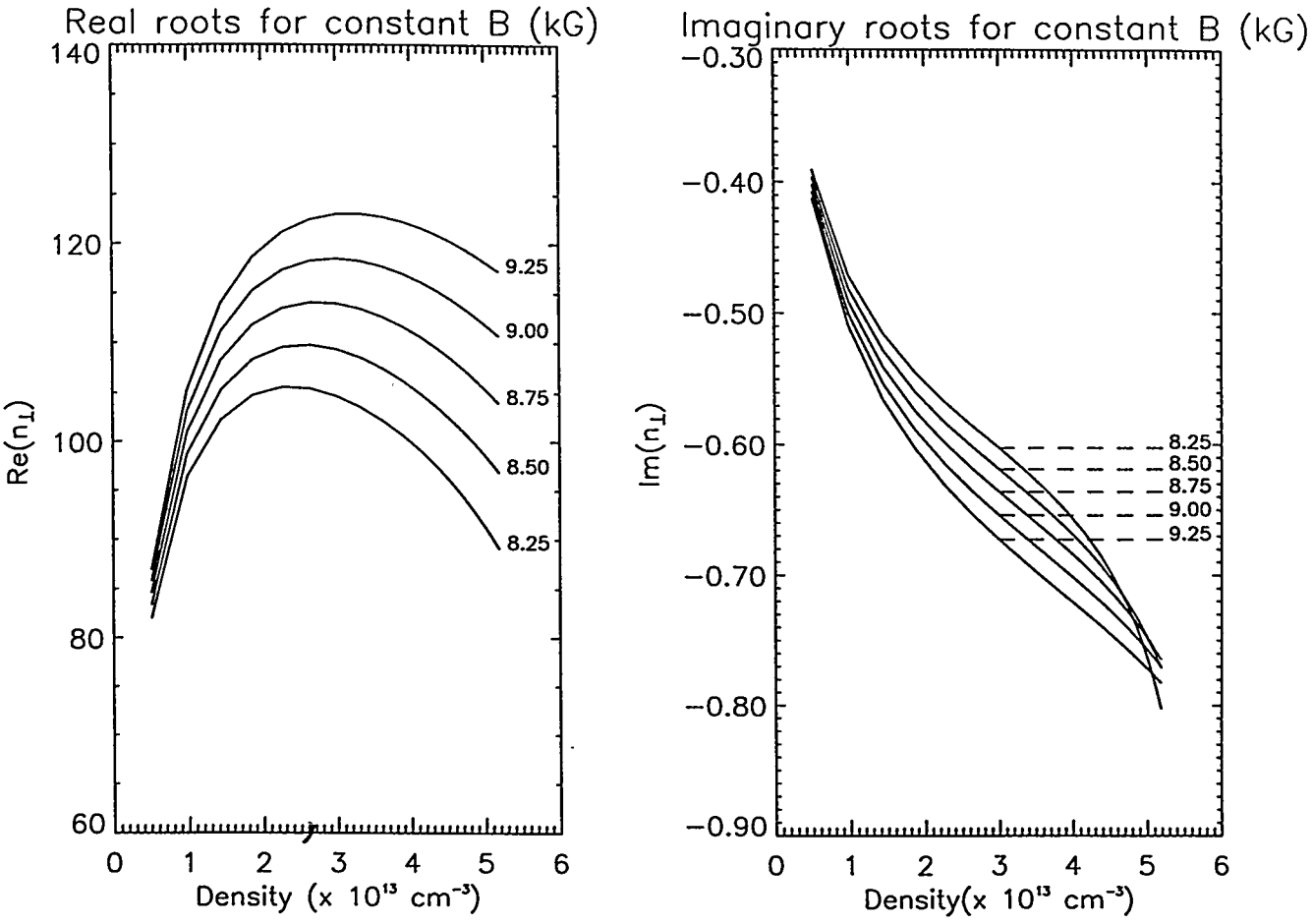

Figure 6: Behavior of the roots of the hot plasma dispersion relation for different values of magnetic field strength. The curves show a monotonically increasing dependence of the roots on $|\boldsymbol{B}|$.

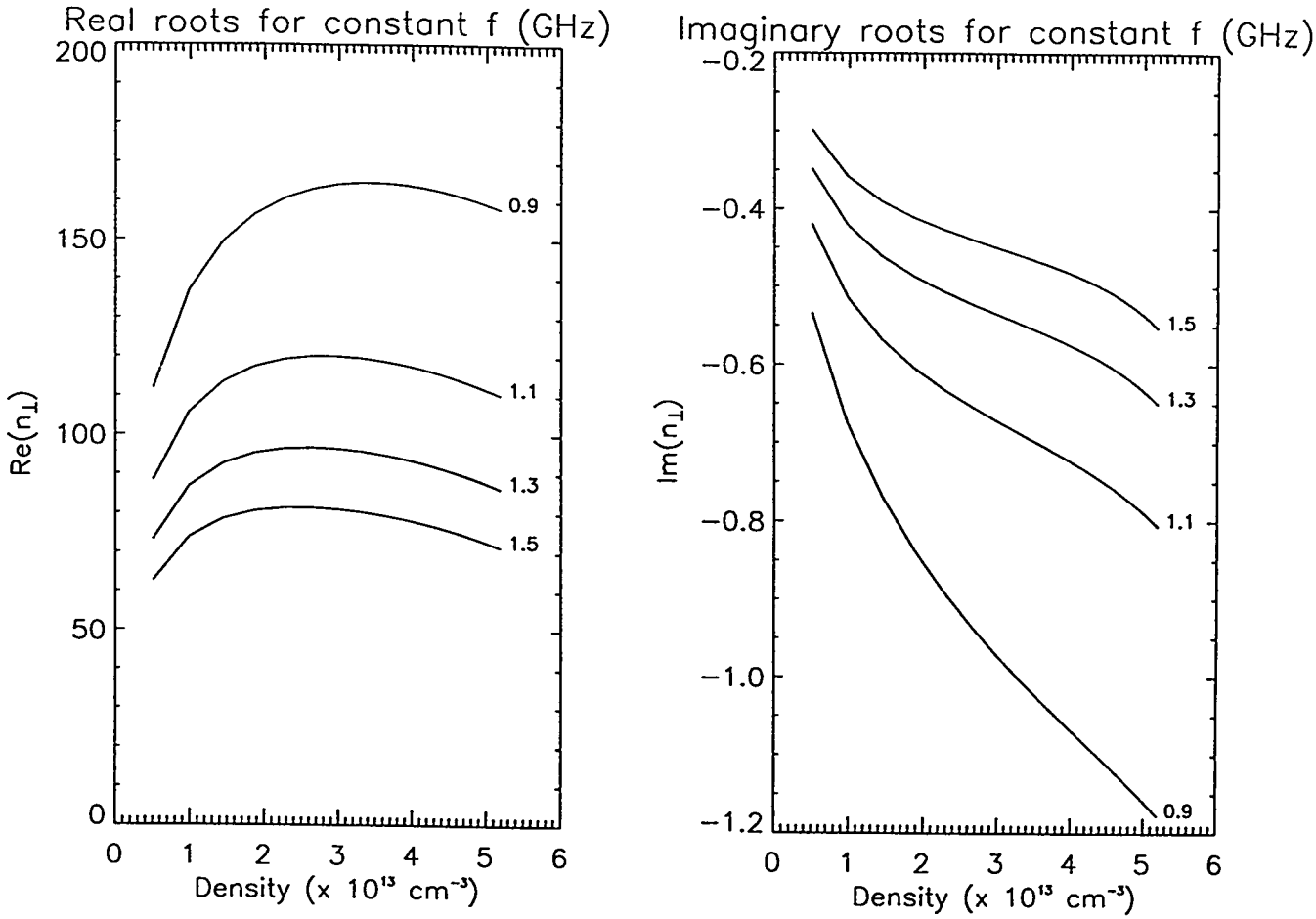

Figure 7: Behavior of the roots of the hot plasma dispersion relation for different values of wave frequency. The real curves indicate an inverse dependence between $n_\perp$ and frequency. Damping increases as the frequency decreases toward the lower hybrid frequency.

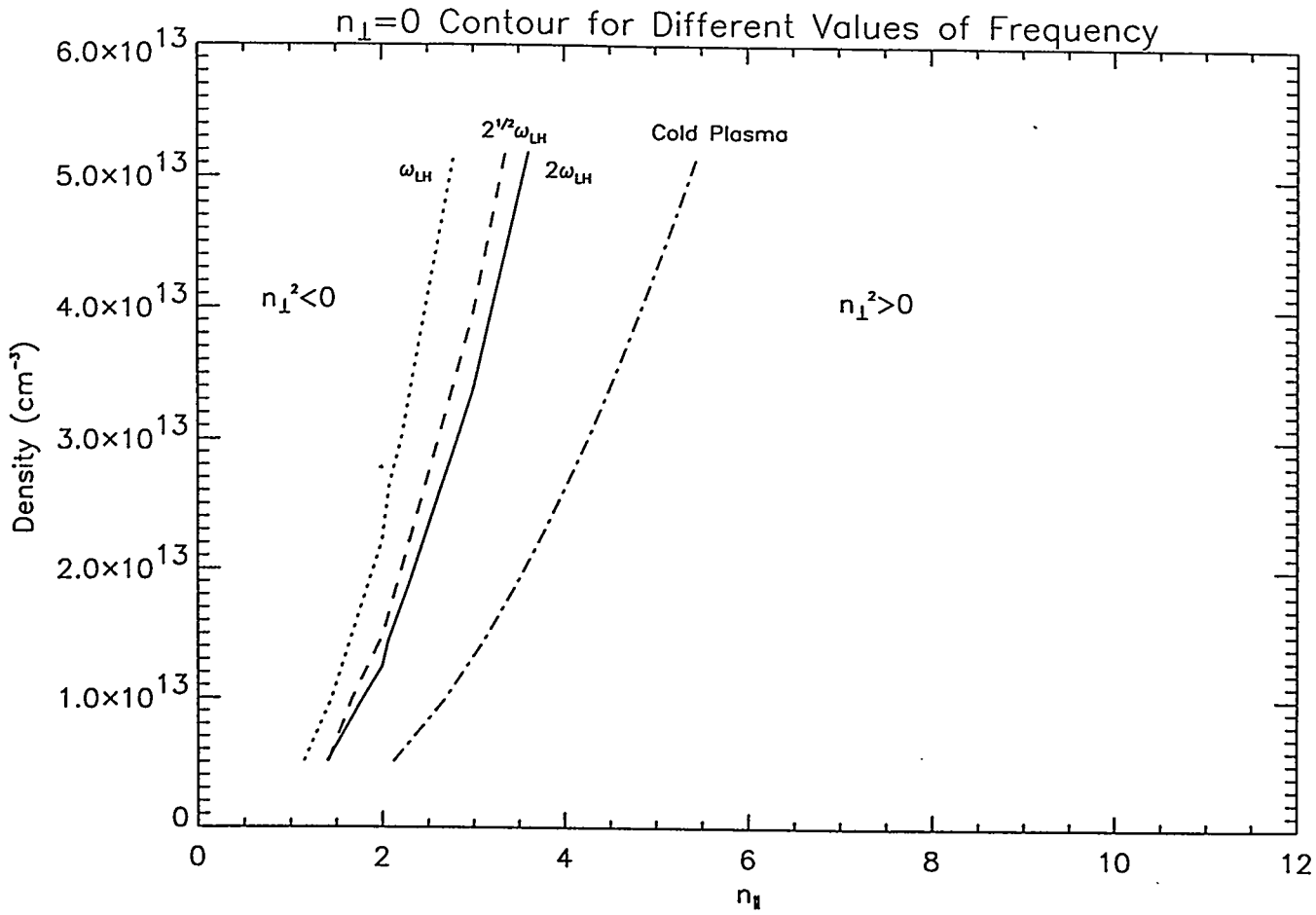

Figure 8: Contour plot of $n_\perp^2 = 0$ for RFX at $I/N = 6\times10^{-14}\ A\cdot m$ and $T \to 0eV$ for different values of wave frequency. Here, dotted lines correspond to $\omega \approx \omega_{LH}$, dashed lines correspond to $\omega \approx \sqrt{2}\omega_{LH}$, and solid lines correspond to $\omega \approx 2\omega_{LH}$. The cold plasma cutoff is also present (dot-dash lines).

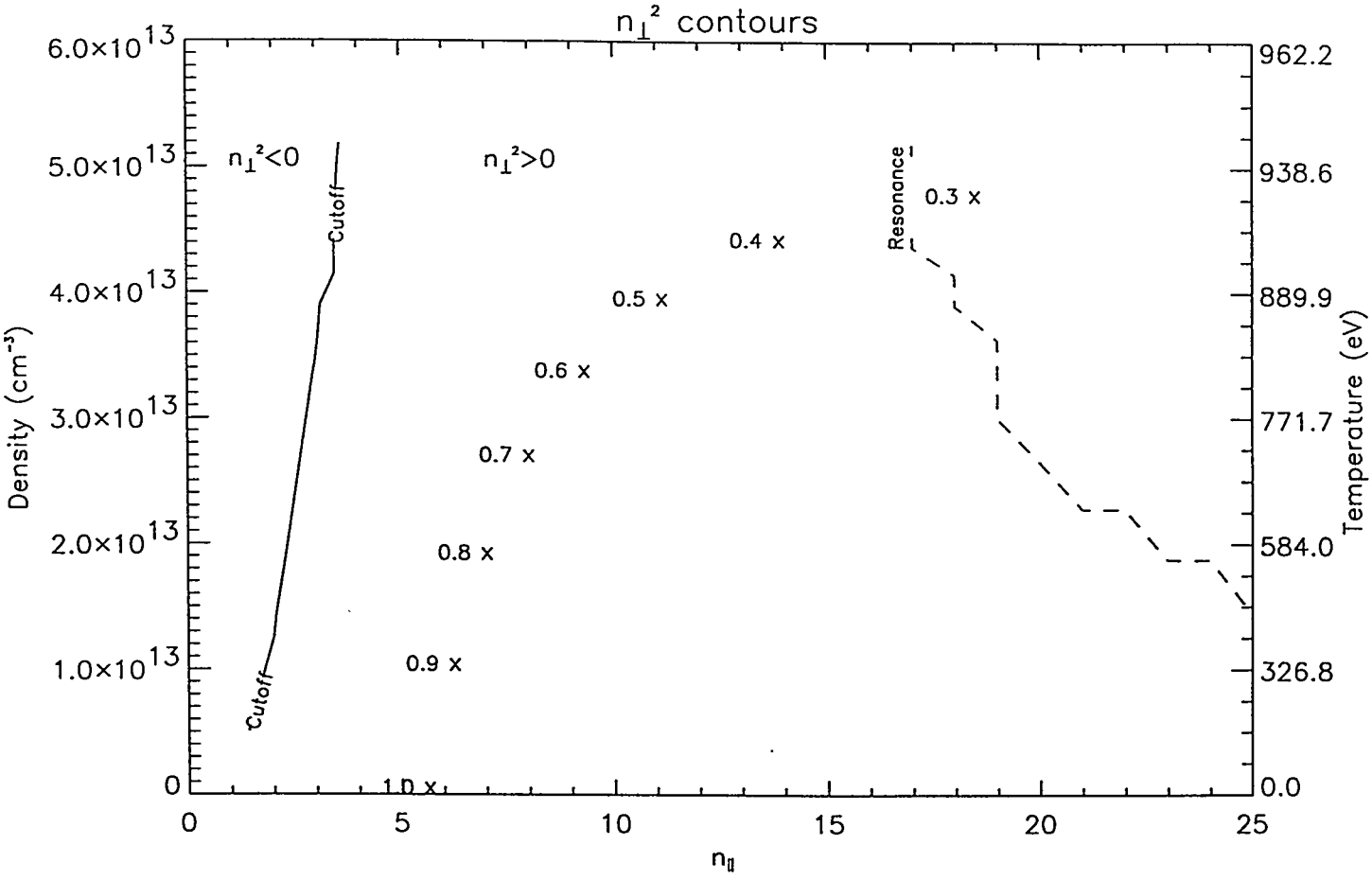

Figure 9: Contour plot of $n_\perp^2 = 0$. The path of the wave through the plasma has been marked by 'x' and labeled with the corresponding r/a value. The dashed curve shows the region of the resonance between the wave parallel phase velocity and the electron parallel thermal velocity.

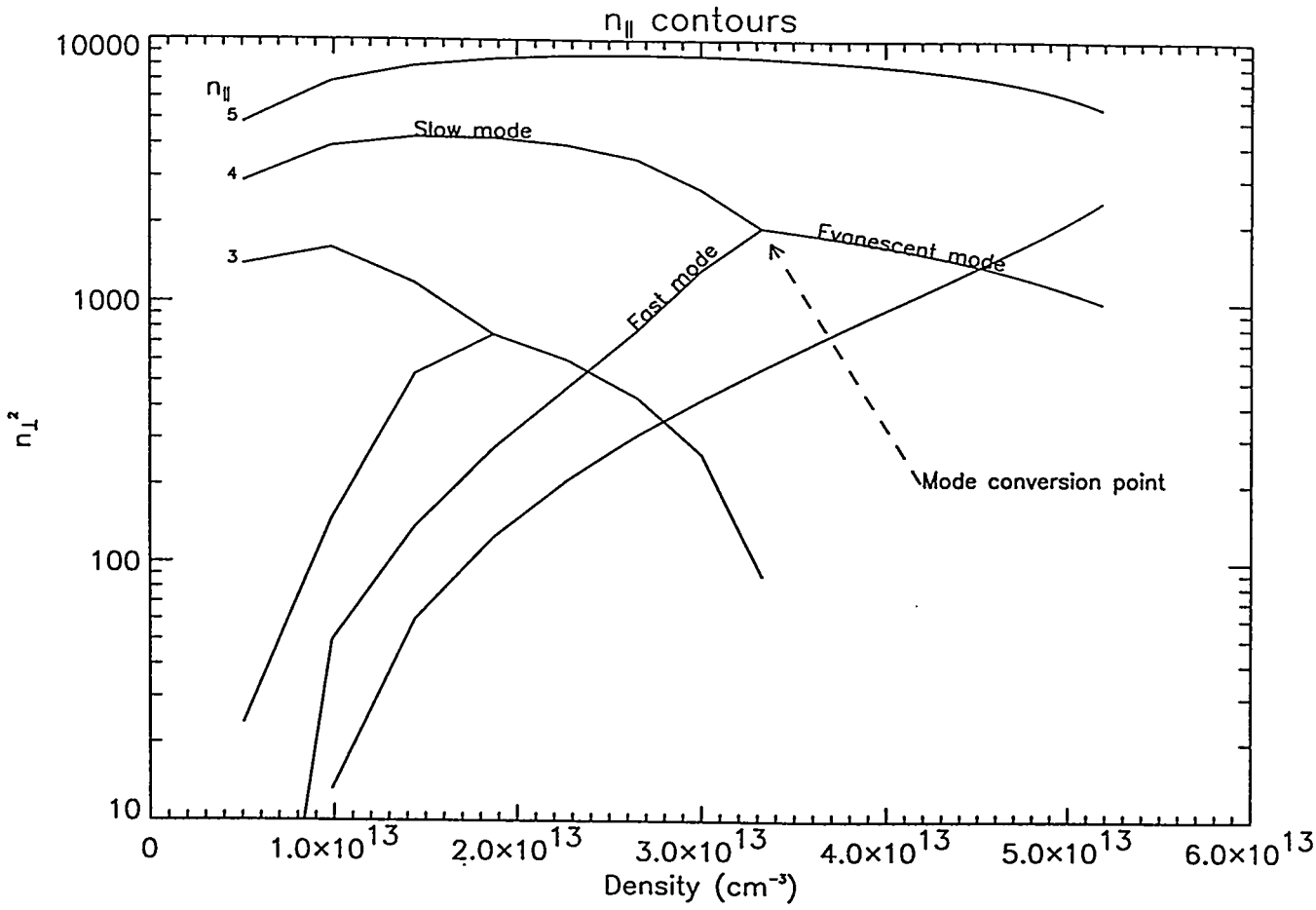

Figure 10: Plots of values of $n_\perp^2$ for the slow and fast wave as density increases for selected values of $n_\parallel$ in RFX. The extra path at the mode conversion point is an evanescent mode inside the cutoff.

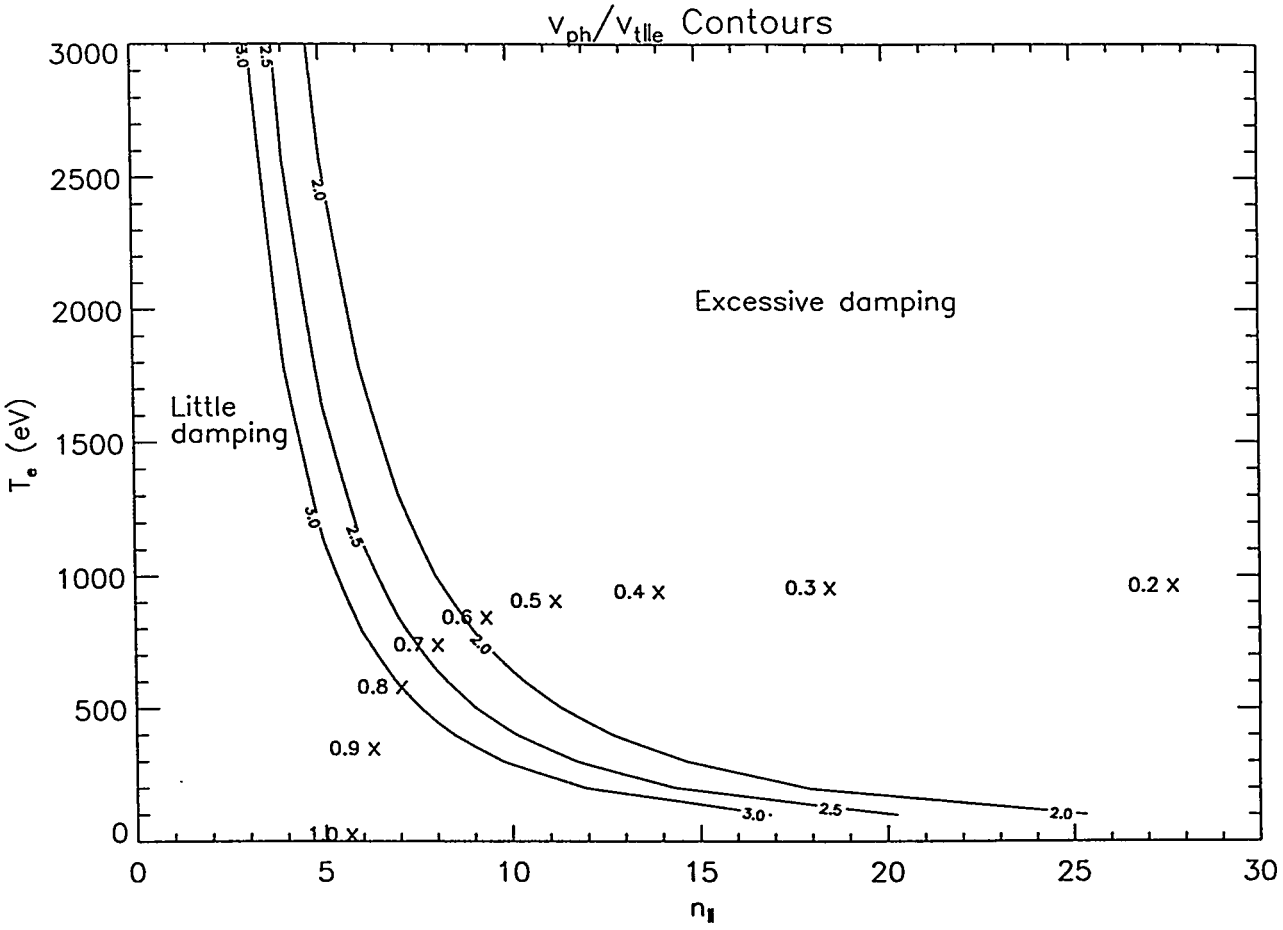

Figure 11: Contours of v_{ph}/v_{tlle} over parallel index of refraction and temperature. Uchimoto predicts that optimal Landau damping occurs where $v_{ph}/v_{tlle} \approx 2.5$. The path of the ray is marked by 'x' and labeled with the corresponding value of r/a. Here, the ray is located for ideal Landau damping in the region $r/a \approx 0.7$.

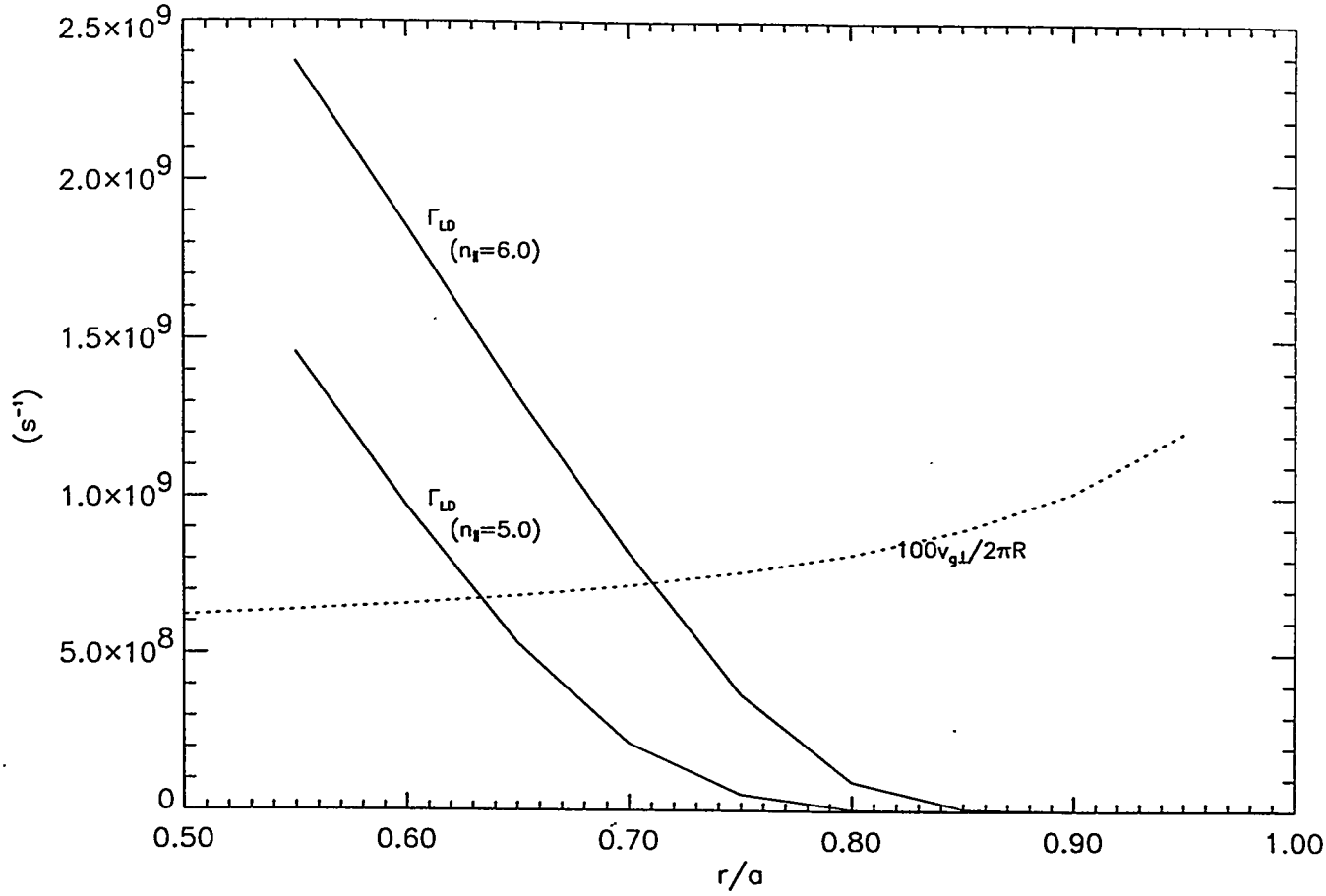

Figure 12: Landau damping rate (solid) versus $100v_{g\perp}/2\pi R$ (dotted) as a function of r/a for the cases of $n_{\parallel edge} = 5.0$ and $n_{\parallel edge} = 6.0$. The point of intersection of the two curves marks the region of ideal Landau damping. Since the two points fall on either side of $r/a = 0.7$, we estimate that the ideal $n_{\parallel edge} = 5.5$.

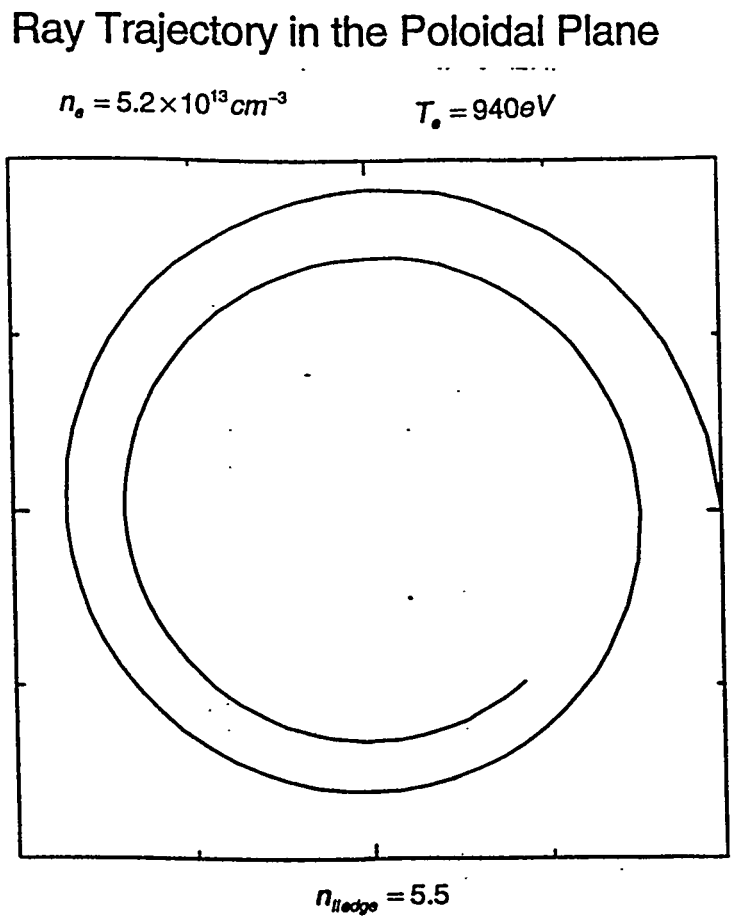

Figure 13: Ray trajectory in a constant toroidal angle plane for RFX where $n_{\parallel edge} \approx 5.5$. The ray is launched at the wall and makes slightly less than two poloidal transits before being completely absorbed by the plasma.

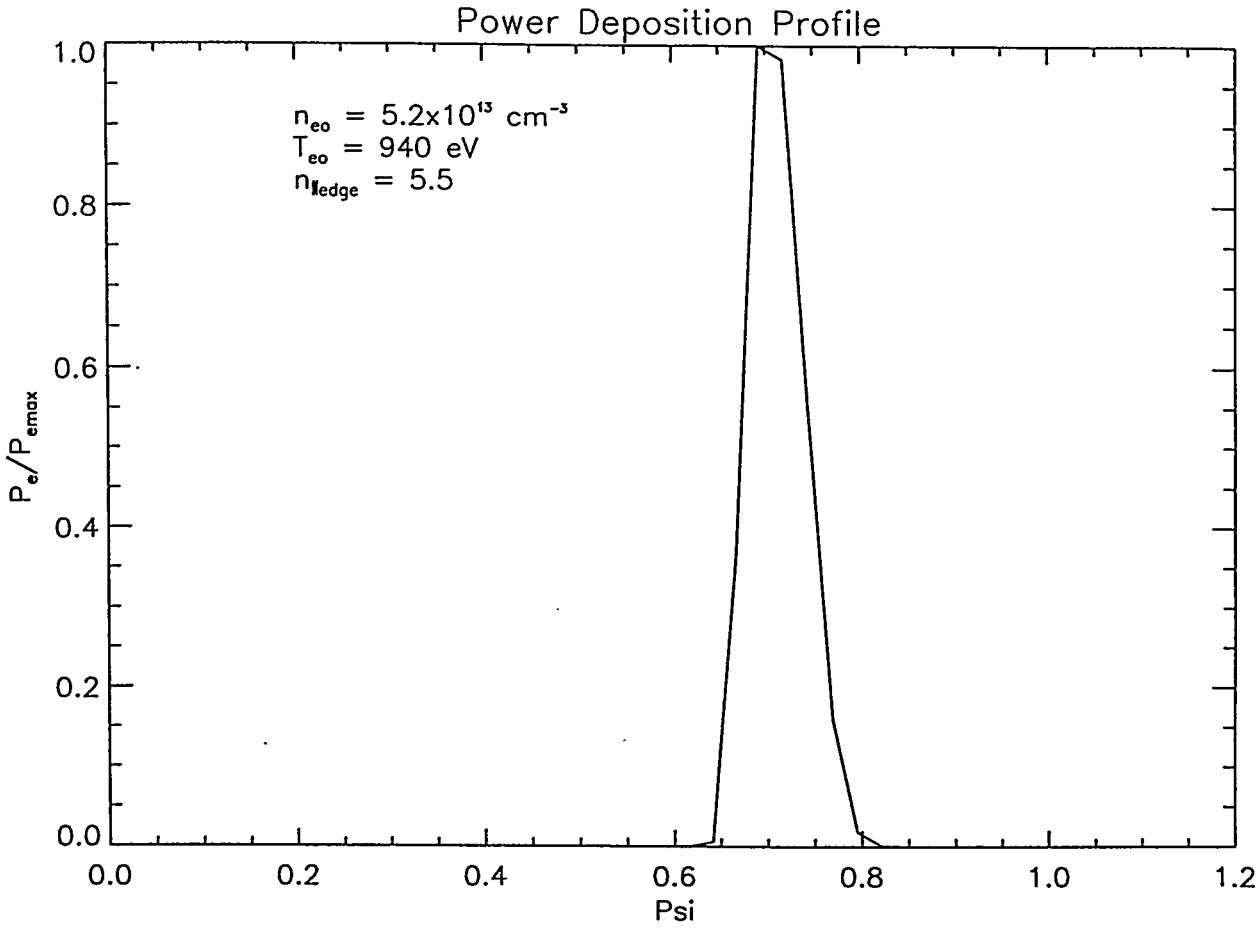

Figure 14: Power deposition profile for the lower hybrid wave launched into RFX with $n_{\parallel edge} = 5.5$. The spike located at $\psi \approx 0.7$ (ψ is a flux surface coordinate analogous to r/a) is indicative of a relatively large amount of power to the electrons at this point and, therefore, of current driven in this region. Power delivered to the ions was negligible.

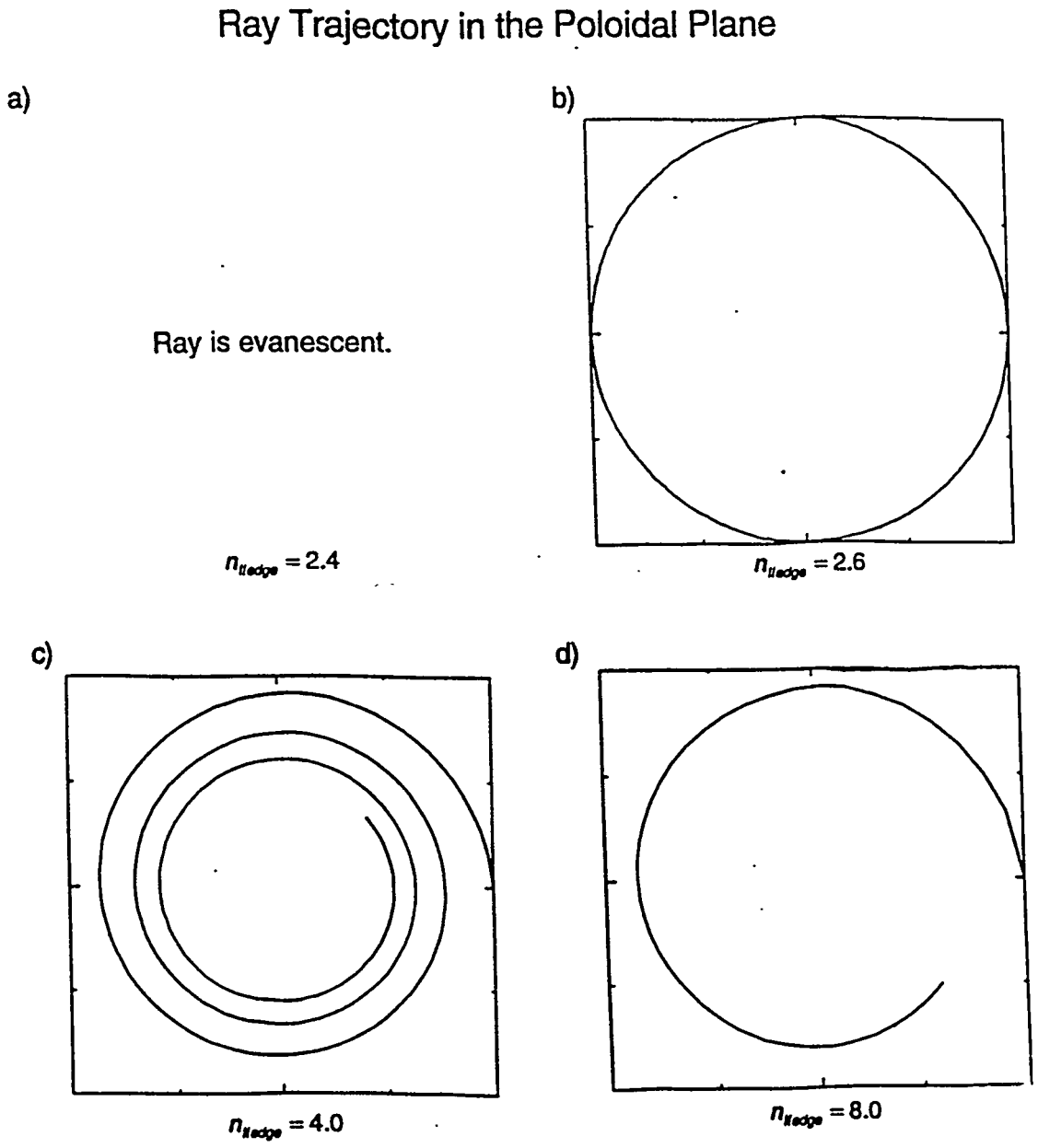

Figure 15: Ray trajectory in a constant toroidal angle plane for RFX where $n_{\|edge}$ is allowed to vary. a) The parallel index of refraction is below the cutoff for the edge density of RFX and the wave is evanescent. b) The parallel index of refraction allows the wave to enter the plasma edge, but not to propagate further. The wave is a surface wave. c) The wave makes just over three poloidal transits for $n_{\|edge} = 4.0$. d) The wave damps out within one poloidal transit for $n_{\|edge} = 8.0$.

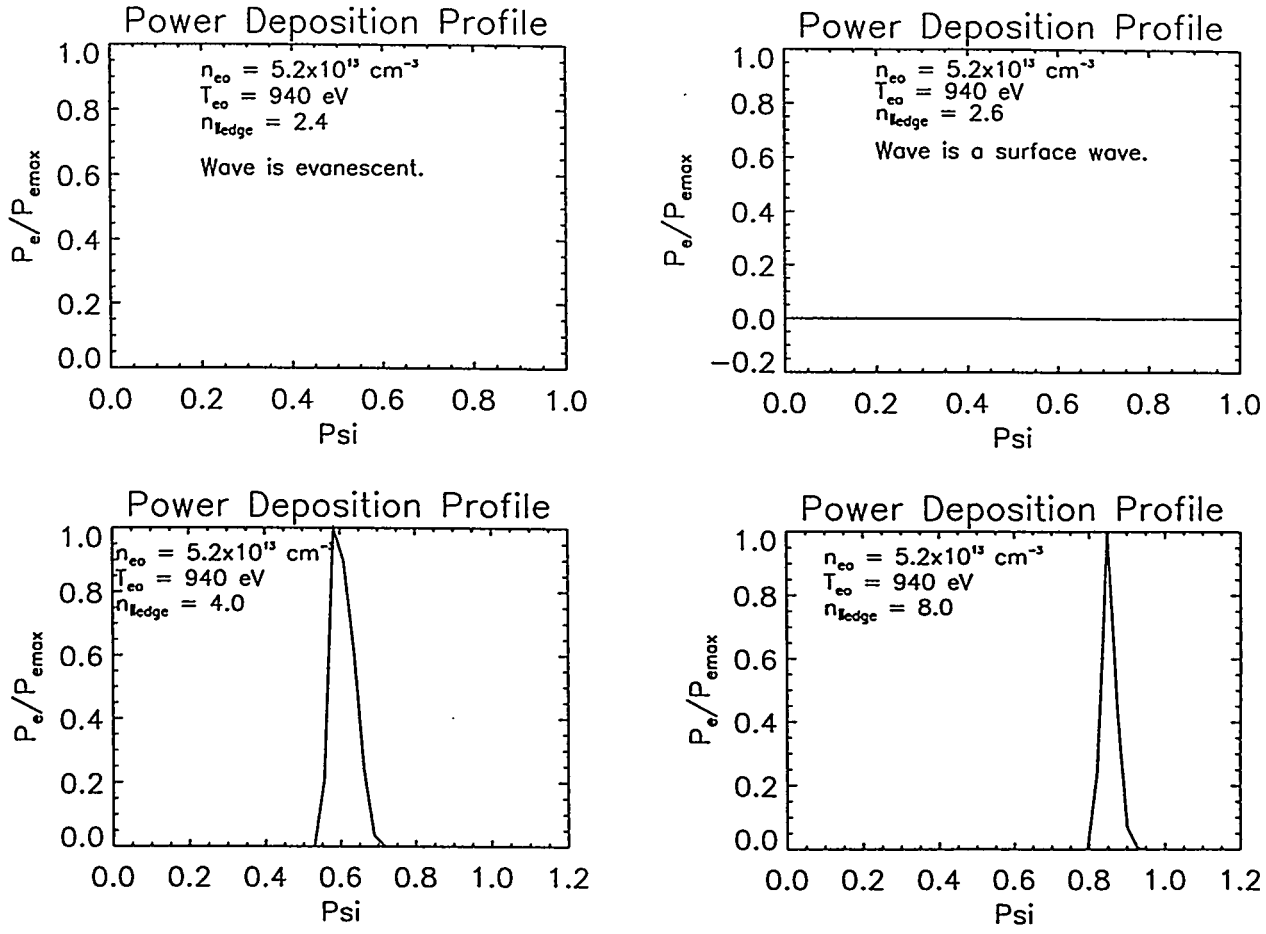

Figure 16: Power deposition profiles for the cases discussed in Figure 15. Note that the electrons receive maximum power at c) $\psi = 0.6$ for $n_{\parallel edge} = 4.0$ and d) $\psi = 0.85$ for $n_{\parallel edge} = 8.0$.

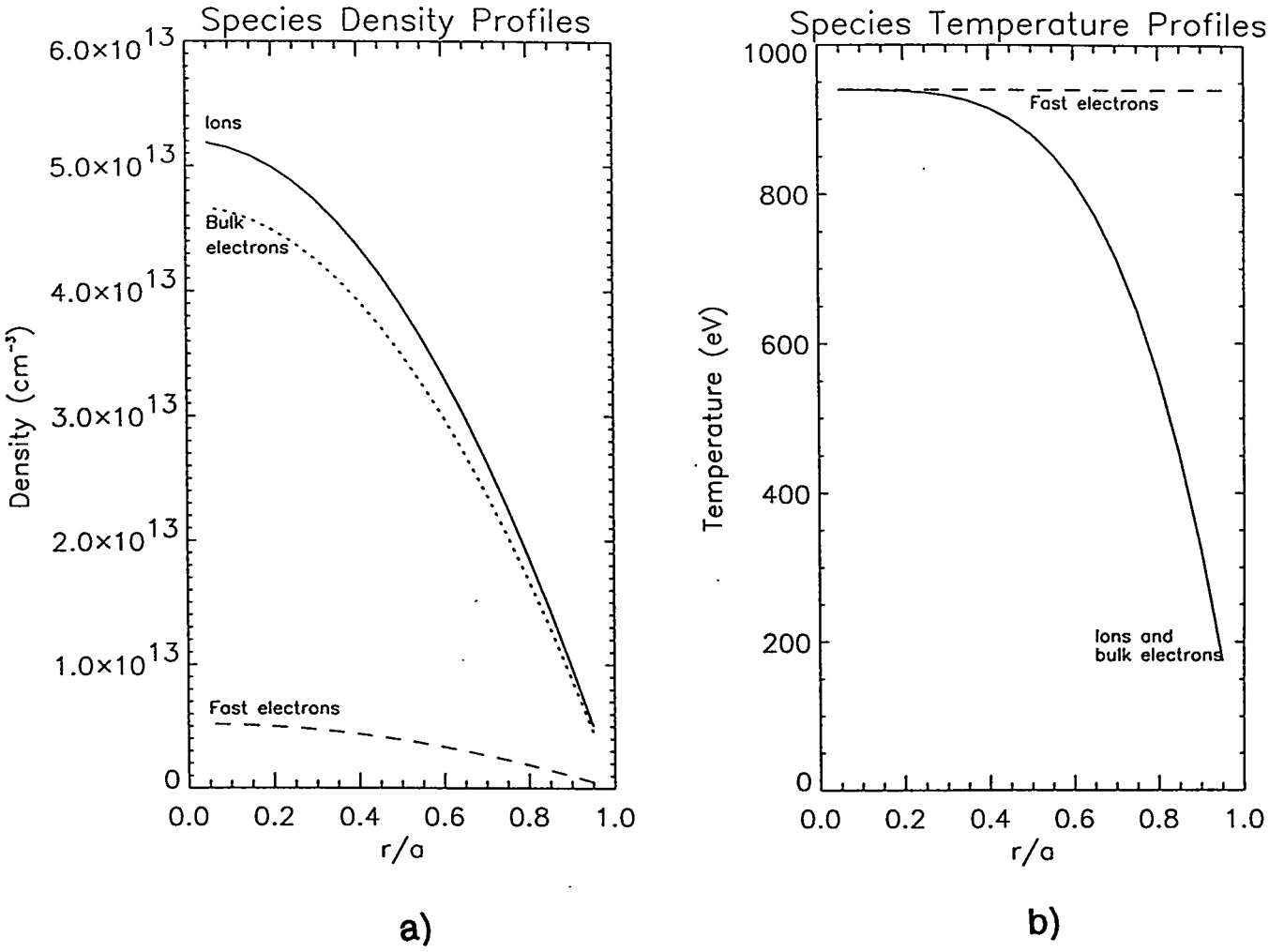

Figure 17: a) Assumed density and b) temperature profiles for RFX with a fast electron species present.

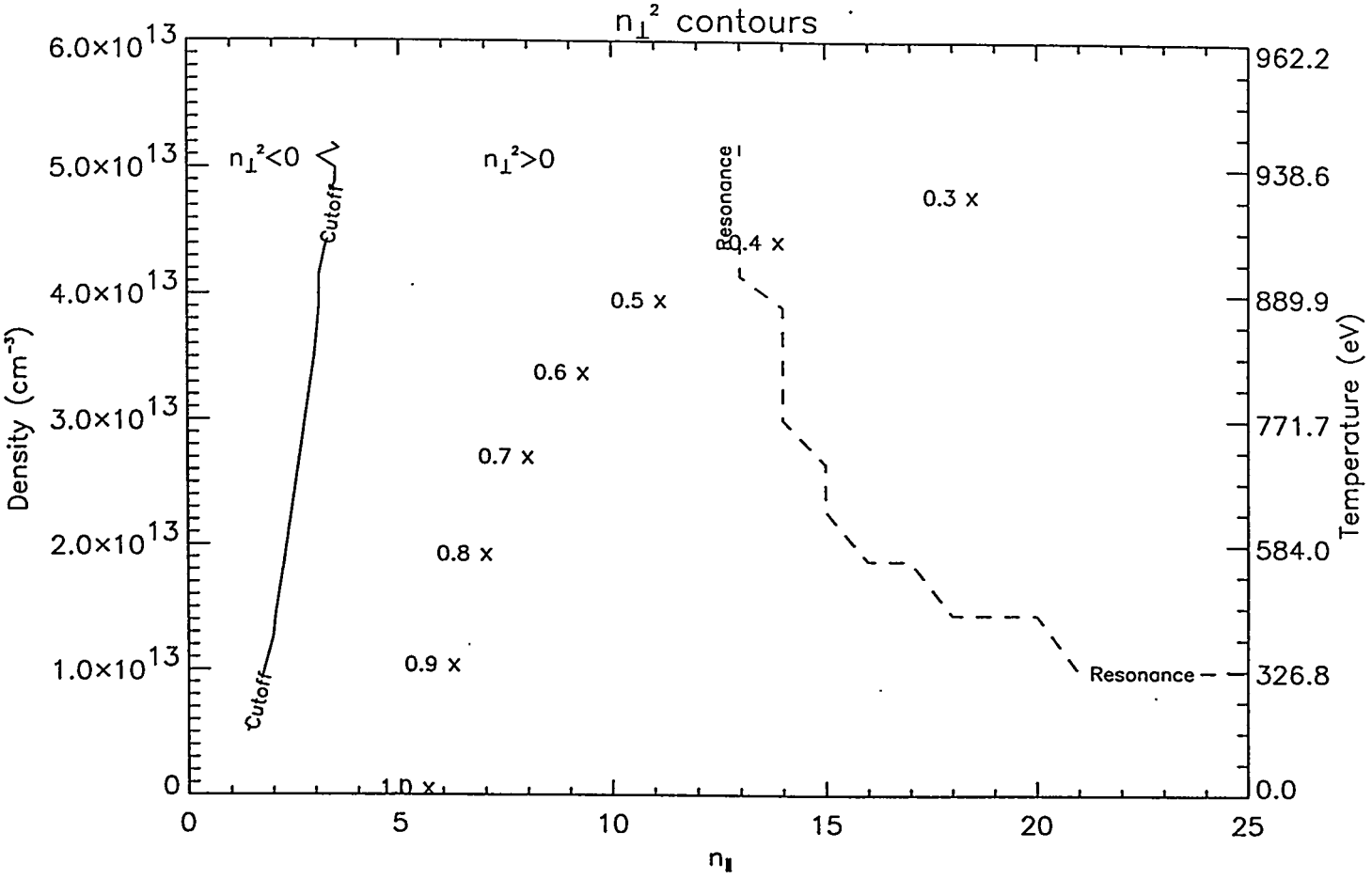

Figure 18: As in Figure 9, but for an RFX plasma with 10% hot electrons. Note that the thermal resonance has shifted to lower $n_{||}$.

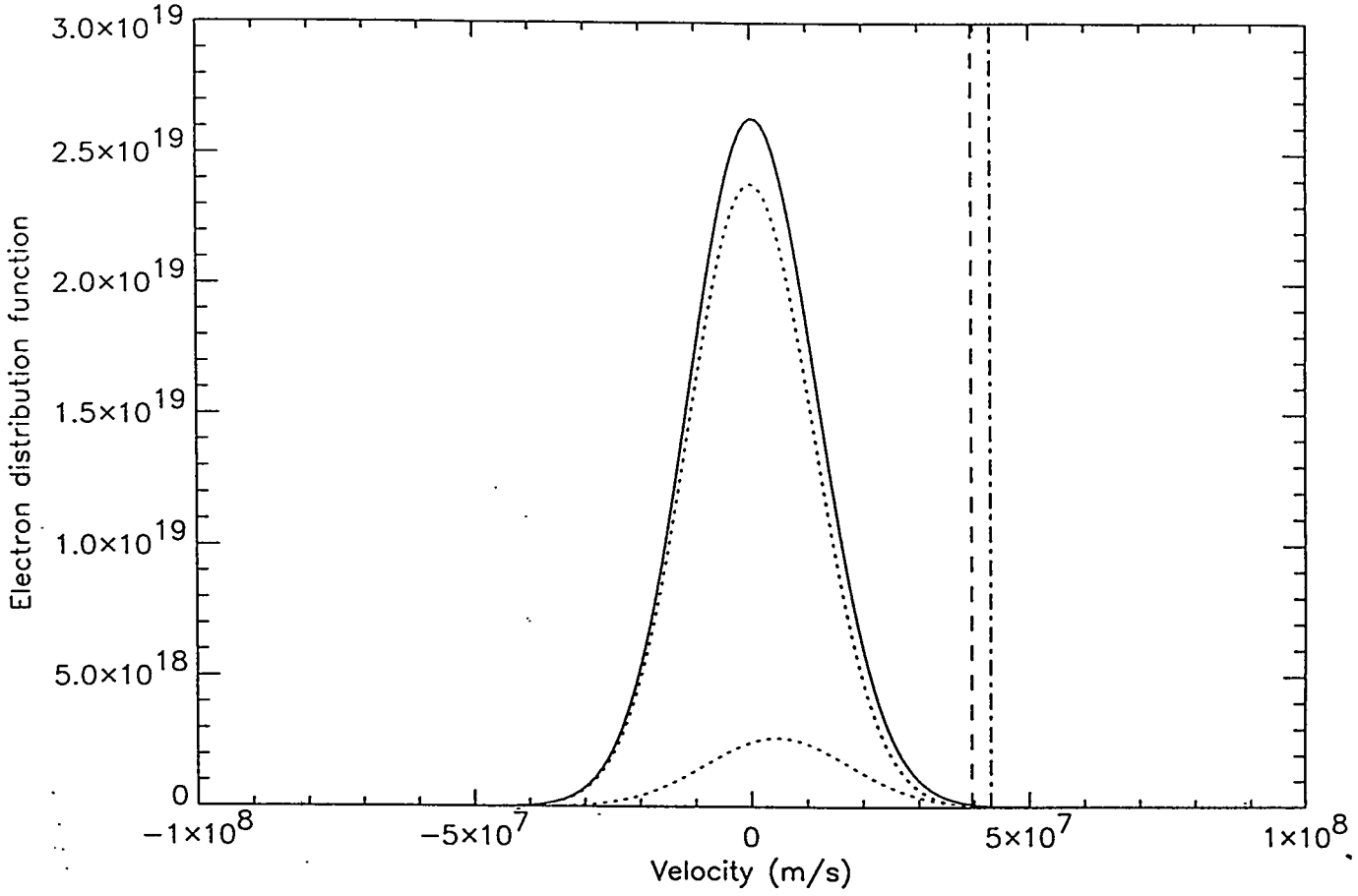

Figure 19: Diagram of the total electron distribution function (solid) and electron species distribution functions (dotted) where the smaller dotted curve represents the fast electrons. The dashed vertical line represents where $v_{ph}/v_{tIIe} \approx 2.5$ (optimal Landau damping) for the case of no hot electrons present. The second vertical line is where the same number of electrons have parallel thermal velocities less than the wave parallel phase velocity for the case of hot electrons present.

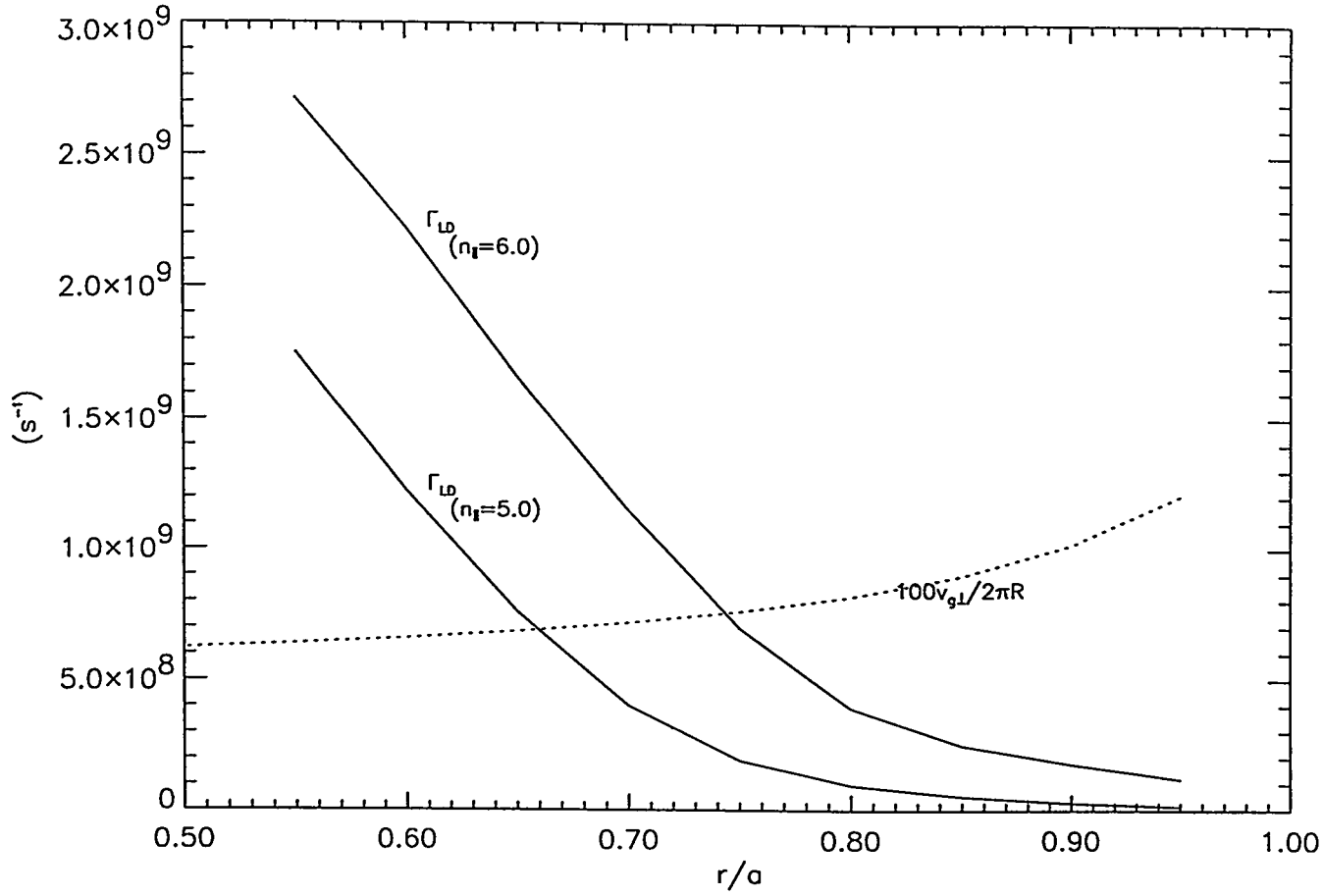

Figure 20: As in Figure 4 but for an RFX plasma with 10% fast electrons. The ideal damping points for each figure have shifted toward the edge of the plasma. To maintain optimal damping, this corresponds to a 6% increase in the wave's phase velocity at the edge of the plasma.

EXTERNAL DISTRIBUTION IN ADDITION TO UC-20

S.N. Rasband, Brigham Young University
T. Dolan, EG&G Idaho, Inc.
R.A. Moyer, General Atomics
J.B. Taylor, Institute for Fusion Studies, The University of Texas at Austin
E. Uchimoto, University of Montana
F.W. Perkins, PPPL
O. Ishihara, Texas Technical University
M.A. Abdou, University of California, Los Angeles
R.W. Conn, University of California, Los Angeles
P.E. Vandenplas, Association Euratom-Etat Belge, Belgium
Centro Brasileiro de Pesquisas Firicas, Brazil
P. Sakanaka, Institute de Fisica-Unicamp, Brazil
Mme. Monique Bex, GANIL, France
J. Radet, CEN/CADARACHE, France
University of Ioannina, Greece
R. Andreani, Associazione EURATOM-ENEA sulla Fusione, Italy
Biblioteca, Istituto Gas Ionizzati, EURATON-ENEA-CNR Association, Italy
Plasma section, Energy Fundamentals Division Electrotechnical Laboratory, Japan
Y. Kondoh, Gunma University, Kiryu, Gunma, Japan
H. Toyama, University of Tokyo, Japan
Z. Yoshida. University of Tokyo, Japan
FOM-Instituut voor Plasmafysica "Rijnhuizen," The Netherlands
Z. Ning, Academia Sinica, Peoples Republic of China
P. Yang, Shandong University, Peoples Republic of China
S. Zhu, University of Science & Technology of China, People's Republic of China
I.N. Bogatu, Institute of Atomic Physics, Romania
M.J. Alport, University of Natal, Durban, South Africa
R. Storer, The Flinders University of South Australia, South Australia
B. Lehnert, Royal Institute of Technology, Sweden
Librarian, CRPP, Ecole Polytechnique Federale de Lausanne, Switzerland
B. Alper, Culham Laboratory, UK
A. Newton, UK

2 for Chicago Operations Office
5 for individuals in Washington Offices

INTERNAL DISTRIBUTION IN ADDITION TO UC-20
80 for local group and file